

České vysoké učení technické v Praze
Fakulta jaderná a fyzikálně inženýrská
Katedra fyzikální elektroniky

Generace vysokých harmonických
frekvencí v hustotně modulovaném
prostředí

High-order harmonic generation in a
density-modulated medium

Diplomová práce

Autor práce: Bc. Matěj Dvořáček
Vedoucí práce: Ing. Jaroslav Nejdrl, Ph.D.
Konzultant(i): Ing. Alexandr Jančárek, CSc.
Ing. Ondřej Finke
Školní rok: 2021/2022

Před svázáním této stránky **vložíte zadání práce** s podpisem děkana (v jedné kopii práce bude list s originálem podpisu).

Toto bude jediný oboustranný list ve Vaší práci!

Prohlášení

Prohlašuji, že jsem předloženou práci vypracoval samostatně a že jsem uvedl veškerou použitou literaturu.

V Praze dne 26. dubna 2022

Matěj Dvořáček

Poděkování

Chtěl bych poděkovat mému vedoucímu Ing. Jaroslavu Nejdlovi, Ph.D. za přívětivý a ochotný přístup. Dále chci poděkovat Ing. Ondřeji Finkemu za trpělivý přístup a jeho cenné rady. V poslední řadě děkuji mé rodině za neustálou podporu během celého studia.

Matěj Dvořáček

Název:

Generace vysokých harmonických frekvencí v hustotně modulovaném prostředí

Abstrakt:

Předmětem studia této práce je generace vysokých harmonických frekvencí v hustotně modulovaném prostředí. Proces generace vysokých harmonických frekvencí je vysvětlen pomocí tříkrokového modelu spolu s podmínkou synchronizace fází. Následně je popsán fyzikální model šíření světla v plynové cele. Na základě fyzikálního modelu je vytvořen kód v programu MATLAB[®], pomocí kterého jsou vypočítány simulace pro generaci vysokých harmonických frekvencí v hustotně modulovaném prostředí. Laserový pulz je navržen vzhledem k výsledkům simulací tak, aby bylo dosaženo selektivní filtrace jediného harmonického řádu. Poté jsou prezentovány experimentální terče za účelem dosažení hustotní modulace v plynu. Poslední část práce je věnována experimentu provedenému ve výzkumném centru ELI Beamlines v Dolních Břežanech.

Klíčová slova:

Generace vysokých harmonických frekvencí, tříkrokový model, synchronizace fází, kvazi-synchronizace fází, hustotní modulace, selektivní filtrace

Title:

High-order harmonic generation in a density-modulated medium

Abstract:

The subject of study of this work is a high harmonic generation in a density-modulated medium. High harmonic generation in a gaseous medium is explained by the three-step model with the condition of phase-matching. This is followed by a description of one dimensional model of light propagation in the gas cell. A code based on the physical model in MATLAB[®] is developed, then simulations of high harmonic generation in density modulated medium are presented. According to the code simulations, a pulse design filtering one harmonic frequency is proposed. After that, experimental density-modulated gas targets are presented. The last part of this work is dedicated to an experiment with a density-modulated gas target realized at ELI Beamlines in Dolní Břežany.

Keywords:

High harmonic generation, Three step model, Phase matching, Quasi-phase matching, Density modulation, Selective filtering

Table of Contents

Introduction	9
1 High harmonic generation	10
1.1 Three-step model	10
1.2 Phase-matching	11
1.2.1 Neutral gas dispersion	11
1.2.2 Plasma dispersion	12
1.2.3 Geometric dispersion	12
1.2.4 Dipole dispersion	13
2 Physical model of high harmonic propagation in a gas	15
2.1 Phase evolution	15
2.2 A combined medium propagation	16
2.3 Medium absorption	18
2.4 Coherence length	18
3 Code implementation in MATLAB[®] for HHG simulations	19
3.1 Pressure modulation calculation	19
3.2 Signal calculation	20
3.3 Analysis of phase and wavenumber	22
3.4 Benchmarking	22
4 Optimalization of single harmonic frequency generation	24
4.1 Ratio of absorption and coherence length	24
4.2 Phase evolution during propagation in the cell	26
4.3 Geometrical dispersion segment of k_0	28
4.4 Ionization η dependence over k_g for sinusoidal modulation	30
4.5 Absorption effect for HHG	33
4.6 Monochromaticity of QPM	35
5 Pulse design for QPM in density modulated target	36
5.1 Ionization by an optical pulse	36
5.2 Dependence of k_g over time t	38
5.3 Beam design	38
5.4 Optical setup	40
6 Density modulated gas targets	42
6.1 Standing acoustic wave	42
6.2 Gas jets	43
7 Experimental implementation of density modulated targets	45
7.1 Description of the experimental setup	45
7.2 Results	47
7.3 Conclusions a discussion	50

Conclusion and discussion	51
References	53
Appendix	54
1 Tables	54
2 MATLAB[®] Codes	55

Introduction

This work concentrates on the high harmonic generation with density modulated targets. It expands and develops work started in [1] and [2]. High harmonic generation is a nonlinear phenomenon offering XUV to soft X-ray source of coherent radiation. Many high harmonic orders are generated as a response of a medium to an ultra-short intense laser pulse. It is desirable for applications to use one of the harmonic wavelengths. Modulating the density of the medium is a method to achieve selective filtering of the harmonic orders during the process. The theoretical design of a density-modulated target allowing selective filtering of single harmonic order is the focus of study in this work.

The first chapter explains the high harmonic generation in a gaseous medium both on the microscopic and macroscopic levels. The second chapter describes the physical model of the light propagation in the gas cell during the generation. Chapter three introduces the numerical implementation of a one-dimensional propagation model from chapter two in MATLAB[®] software. The results of the implemented code for density modulated targets are presented in chapter four. Chapter five focuses on the pulse design for a single high harmonic frequency filtering. Possible experimental methods how to create a density-modulated target are shown in chapter six. The last chapter of this work presents the results of an experiment with a density-modulated target conducted at the research facility ELI Beamlines in Dolní Břežany.

1 High harmonic generation

High harmonic generation (HHG) is a method to produce temporally and spatially coherent extreme-ultraviolet radiation. This phenomenon is a result of focusing high-intensity laser into a medium that is capable of such generation. A typical laser used for this process is an infrared laser with a pulse duration of the order of tens of femtoseconds. The intensity of the laser needs to be in the range of $10^{14} - 10^{15} \text{ W/cm}^2$. In this work a noble gas is considered as the medium that is used for the generation, an example of a typical experimental setup is seen in figure 1. The process is explained by the three-step model that is composed of ionization, propagation of free electron, and recombination. Apart from the three-step model which explains the generation on a microscopic level, it is crucial that the phase-matching (PM) condition is fulfilled. We will see that in order to accomplish selective filtering of high harmonic orders we need to achieve a quasi-phase-matching (QPM) condition that will be explained.

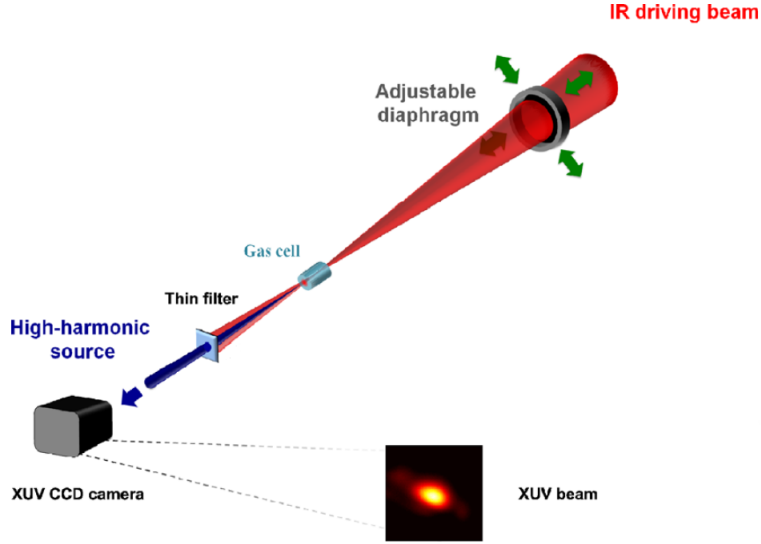


Figure 1: Scheme of high harmonic generation in gas medium, taken and modified from [3]

1.1 Three-step model

The three-step model explains HHG on a microscopic scale. The first step is ionization in which the strong laser field disrupts the Coulomb potential of an atom which leads to ionization. There are three types of ionization - multiphoton ionization, tunneling ionization, and barrier-suppression ionization. The *Keldysh parameter*

$$\gamma_K = \sqrt{\frac{I_p}{2U_p}} \quad (1)$$

is used to distinguish between the types of ionization. When γ_K is much higher than 1 then the atom is ionized by the multiphoton ionization regime. If $\gamma_K \ll 1$ the tunneling regime and barrier ionization occur. The ionization energy I_p and ponderomotive potential

$$U_p = \frac{e^2 E_0^2}{4m_e \omega_0^2} \quad (2)$$

is used to determine γ_K . We see that U_p is dependent on the intensity of EM field E_0^2 and the angular frequency of the laser ω_0 , e is the electron charge, and m_e its mass. The Keldysh parameter grows with higher angular frequencies of the laser and the duration needed for the tunneling gets close to the period of the optical field so the electron does not have enough time to tunnel through the barrier. The free-electron propagating through a continuum and interacting with the laser field is the next step in the model. The last step of the model is the recombination of the electron with its parent ion. When the free-electron recombines, excessive energy is emitted as a high-energy photon. The energy of the photon depends on the ionization potential I_p of the atom and the kinetic energy E_k which is accumulated when the electron propagates in the continuum. We find out by the numerical solution of the trajectory equations that there is a maximum of the kinetic energy the electron can gain $E_k = 3.17 U_p$ where U_p is the ponderomotive potential. The phase of such electron with the highest energy is then used to divide the trajectories into two groups. The *short trajectories* are when the electron leaves the atom in a time after the highest-energy electron is detached and *long trajectories* are reserved for electrons born before this time. The highest energy also defines the *cut-off energy* or *cut-off order* which is the last order that will be generated.

1.2 Phase-matching

The phase-matching condition (PM) is a fundamental criterion for many non-linear optical phenomena and high harmonic generation is no exception. It is essential to maintain a certain phase relationship between the original and generated radiation. We can describe the phase relationship by a phase mismatch number

$$\Delta k_q = k_q - qk_0 = \Delta k_n + \Delta k_e + \Delta k_g - K_{dip}, \quad (3)$$

where k_q is the wavenumber of generated radiation, k_0 is the wavenumber of the driving field, and q is the harmonic order. The phase mismatch wave-number (3) should be equal to or close to zero in order to achieve effective HHG. PM condition depends on factors such as a dispersion of neutral atoms Δk_n , dispersion of plasma Δk_e , geometrical dispersion Δk_g , or harmonic dipole phase that varies in space $K_{dip} = \text{grad } \varphi_{dip}$. The individual factors of (3) are described below.

1.2.1 Neutral gas dispersion

The refractive index n changes with the incident light angular frequency ω and each harmonic order $\omega_q = q\omega_0$ experiences a different propagation speed. We write for the

neutral gas mismatch vector

$$\Delta k_n(\omega_0, q) = k_q - qk_0 = \frac{q\omega_0}{c} [n(q\omega_0) - n(\omega_0)]. \quad (4)$$

The refractive index $n(\omega)$ of noble gases is bigger than 1 for infrared and visible light while it is lower than 1 for light in the soft X-ray region. The refractive indices in the range of infrared light are tabled with the use of the Sellmeier equation which utilizes experimental data for the infrared light. The evaluation of the refractive indices for the extreme ultraviolet radiation is done according to the equation (3.9) in [4].

1.2.2 Plasma dispersion

Just as the refractive index n is the function of wavelength¹ λ for neutral atoms of gas, it also changes for plasma. The refractive index of plasma is defined as [5]

$$n_e(\omega_0) = \sqrt{1 - \frac{\omega_p^2}{\omega_0^2}} = \sqrt{1 - \frac{N_e e^2}{\varepsilon_0 m_e \omega_0^2}}, \quad (5)$$

where N_e is the density of electrons, e is the electron charge, m_e is the electron mass, ε_0 is the vacuum permittivity and ω_0 is the angular frequency of the laser. The electric field in the plasma forces the electrons to oscillate with plasma frequency $\omega_p = \sqrt{\frac{N_e e^2}{\varepsilon_0 m_e}}$.

The plasma frequency ω_p is also limiting frequency for the propagation of radiation with frequency ω as the electromagnetic wave with frequency ω lower than ω_p cannot propagate in plasma. In that case the refractive index (5) is imaginary if $\omega_p > \omega$ and the incident radiation is damped in the plasma. If we take the assumption of laser frequency being much higher than the frequency of the plasma we can write the approximation [1]

$$\Delta k_e(\omega_0, q) = \frac{q\omega_0}{c} (n_e(q\omega_0) - n_e(\omega_0)) \approx \frac{\omega_p^2 (q^2 - 1)}{2\omega_0 c q}. \quad (6)$$

1.2.3 Geometric dispersion

Another element of dispersion comes from a geometry of beam propagating through space. This element depends on the type of the used beam. One would think that the geometry of the beam will not bring any change to the difference of the wavenumbers Δk_q since the generated light copies the properties of the driving field.

In an example of a Gaussian beam, the geometrical change depends on the Gouy phase φ_G which is different for each wavelength and induces a difference between fields Δk_g . We consider the Gouy phase of the Gaussian beam [6]

$$\varphi_G = \arctan \left(\frac{z}{z_R} \right), \quad (7)$$

¹Equally angular frequency ω_0

where

$$z_R = \frac{\pi w_0^2}{\lambda} \quad (8)$$

is the Rayleigh range defined with wavelength λ and the waist radius w_0 . It is a phase difference from a plane wave and it is acquired along the beam propagation z nearby the position of the beam focus. The overall change of the phase for a Gaussian beam going through the focus is π . The Gouy phase appears in the wavenumber k as the derivative according to z

$$k_g = \frac{d}{dz} \left(\arctan \left(\frac{z-x}{z_R} \right) \right) = \frac{z_R}{z_R^2 + (z-x)^2}, \quad (9)$$

where x is the shift of the focus from the origin of coordinates. Overall the geometrical mismatch number Δk_g will depend on the change of the Rayleigh range $z_R(\lambda)$ of the harmonic beam is q -times larger and often the harmonic beam is considered as a plane wave and only the geometrical phase of the driving field is considered.

One of the alternatives to the generally used Gaussian beam is a Bessel beam. Bessel beam is the exact solution of the Helmholtz equation in cylindrical coordinates. However, a true Bessel beam cannot be generated in practice because it would be a plane waveform with infinite energy. In the experimental implementations, the approximation of a Bessel beam is often created by axicons from a Gaussian beam, schemed in figure 2. This Bessel-Gaussian (BG) beam has a transversally inhomogenous distribution of intensity depending on the order of the Bessel function. More importantly for the goals of this work, the BG beam has a resulting geometric wave vector heading in the direction of the propagation in the focus. That is because the wave vectors form a cone around the propagation axis with the same inclination angle.

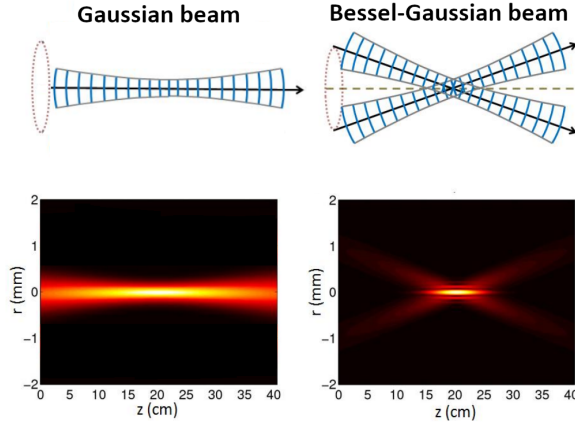


Figure 2: Generation of Bessel-Gaussian beam, taken and modified from [7]

1.2.4 Dipole dispersion

The last segment that contributes to the phase-matching is the dipole phase. In the microscopic model, the electrons propagating through the continuum have different

trajectories for the same kinetic energy causing the phase difference due to different recombination times. The dipole contribution is a negative product of the intensity I and the proportional constant $\alpha_{q,T}$

$$\varphi_{q,dip} = -\alpha_{q,T}I. \quad (10)$$

The proportional constant $\alpha_{q,T}$ differs for long trajectories $T = L$ and short trajectories $T = S$. The proportional constant $\alpha_{q,T}$ is positive for short trajectories and negative for long trajectories and it depends on the intensity and wavelength of the laser $\alpha_{q,T} \propto \frac{1}{I_0\lambda_0}$ [8]. The dipole phase mismatch number is the derivative of the intensity

$$K_{dip} = -\alpha \frac{dI}{dz} \quad (11)$$

along the direction of the propagation z .

2 Physical model of high harmonic propagation in a gas

In an attempt to understand the evolution of the harmonic signal in the gas cell we need to get an insight into the light propagation in general medium. This means to describe the medium with a refractive index $n(z)$. The medium alone is composed of neutral atoms of noble gas and plasma. This chapter explains the physical model describing signal evolution used later for numerical simulations.

2.1 Phase evolution

The light phase evolves during propagation throughout the medium. The phase evolves for both the laser beam and generated radiation and at the end of the medium of length L corresponds to [9]

$$\varphi = \int_0^L k(z) dz, \quad (12)$$

where k is the wavenumber and z is the on-axis coordinate. If we suppose that the light is described as $\vec{E} = \vec{E}_0 e^{i\psi}$ at the beginning of the medium, then the light is in state $\vec{E} = \vec{E}_0 e^{i(\psi+\varphi)}$ after the propagation.

The gas cell is filled with particles and the laser beam propagates through each point of the cell. Therefore, at each point of the cell the harmonic field is generated. This works for all generated orders but the evolution will be described only for single harmonic order q . To describe single harmonic order, equation (12) needs to be modified since the phase is firstly affected by propagation of the laser to the point z by the laser and secondly by propagation of the HH field to the end of the medium

$$\varphi_q(z, L) = q \int_0^z k_0(z') dz' + \int_z^L k_q(z') dz' \quad (13)$$

where k_0 is the laser wavenumber and k_q is the HH wavenumber of order q . This is the phase of harmonic field at the end of the medium generated at position z . There are N points in the cell. We then write for the field originating at each point

$$\begin{aligned} \varphi_{q1} &= q \int_0^{z_1} k_0(z') dz' + \int_{z_1}^L k_q(z') dz' \\ \varphi_{q2} &= q \int_0^{z_2} k_0(z') dz' + \int_{z_2}^L k_q(z') dz' \\ &\vdots \\ \varphi_{qN} &= q \int_0^{z_N} k_0(z') dz' + \int_{z_N}^L k_q(z') dz' \end{aligned} \quad (14)$$

and the field for the order q at the end of the cell is a sum of high harmonic signals from each point of the medium

$$E_q(L) = \sum_{j=1}^N \exp(i \varphi_{qj}(z_j, L)), \quad (15)$$

where we have considered a constant amplitude of the field. The illustration of high harmonic signal propagating in a cell is presented in figure 3.

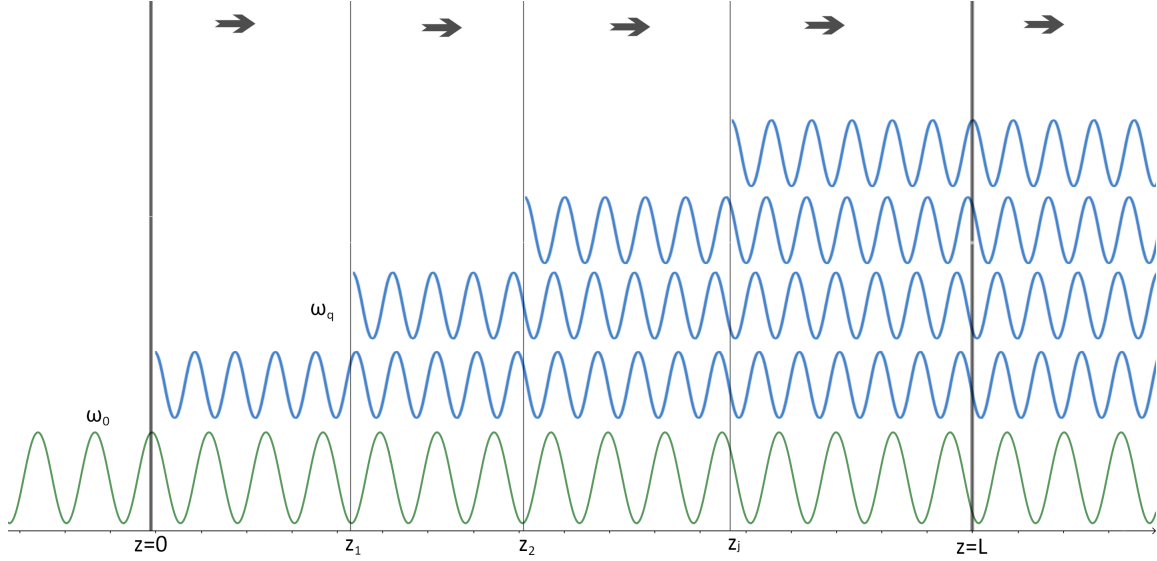


Figure 3: Illustration of laser propagating through medium and generating high harmonic frequencies

2.2 A combined medium propagation

As we have seen in chapter 2.1, the phase of the HH field along the medium plays a fundamental role. We were able to see from equation (13) that the phase is calculated using the wavenumber of laser radiation k_0 and the wavenumber of the high harmonic radiation k_q . Since the high harmonic generation happens in the gas cell filled with neutral atoms of noble gas and plasma created by the high-intensity laser, we need to calculate wavenumbers k_0 , k_q in order to define the newborn high harmonic field E_q . This may be achieved through the additivity of electric susceptibility χ [10]

$$k = \frac{2\pi}{\lambda'} = \frac{2\pi}{\lambda} \sqrt{\chi + 1} = \frac{2\pi}{\lambda} \sqrt{\chi_n + \chi_e + 1}. \quad (16)$$

The electric susceptibility of neutral atoms has the dependence $\chi_n = \chi_n(\lambda)$ and the electric susceptibility of plasma has the dependence $\chi_e = \chi_e(\lambda, \eta)$, where η is the percentage of ionized atoms in the cell². The electric susceptibility of plasma is calculated by the relation

$$\chi_e(\omega_0, \eta) = n_e^2 - 1 = -\frac{\omega_p^2}{\omega_0^2} = -\frac{\eta N e^2}{m_e \epsilon_0 \omega_0^2}, \quad (17)$$

that was is derived from (5) and N is the density of neutral gas atoms. The susceptibility of neutral gas can be obtained from the formula

$$\chi_n(\lambda) = n_n^2(\lambda) - 1, \quad (18)$$

²We presume both χ_n, χ_e to be evaluated in atmospheric pressure

where the refractive index is a function of λ . The tables of the refractive index for certain wavelengths may be found at [11].

A case of high harmonic generation in a periodically modulated medium will be considered in later sections. The inhomogeneous gas density needs to be addressed in the definition of wavenumber k . For this reason, a ratio of pressure in the gas cell $p(z)$ and atmospheric pressure p_a defines the modulation. The combined susceptibility with the ratio $p(z)/p_a$ is scaled as follows

$$k = \frac{2\pi}{\lambda} \sqrt{\frac{p(z)}{p_a} \left(\chi_e(\lambda, \eta) + (1 - \eta)\chi_n(\lambda) \right) + 1}, \quad (19)$$

where the factor $(1 - \eta)$ is used to maintain the relation of ionized and neutral gas. The geometrical wavenumber for the Gaussian beam is added as (9) with the origin of coordinates set at the start of the cell $z = 0$. Furthermore, there is a dipole contribution in the wavenumber of the generated field that is based on the intensity I distribution in the cell. For the Gaussian beam, we have [12]

$$I(r, z) = I_0 \left(\frac{w_0}{w(z)} \right)^2 \exp \left(-\frac{2r^2}{w(z)^2} \right), \quad (20)$$

where w_0 is the waist radius, w is the radius of the beam at the plane z along the beam, r is the radial distance from the center axis of the beam and I_0 is the intensity at the center of the beam at its waist. The intensity (20) is reduced in one dimension along the axis of the beam to

$$I(z) = I_0 \left(\frac{w_0}{w(z)} \right)^2 = \frac{I_0}{1 + \left(\frac{z-x}{z_R} \right)^2}. \quad (21)$$

The dipole wavenumber addition is proportional to the derivative according to z of the intensity

$$k_{dip} = -\alpha \frac{d}{dz} \left(\frac{I_0}{1 + \left(\frac{z-x}{z_R} \right)^2} \right) = 2\alpha I_0 z_R^2 \frac{z-x}{(z_R^2 + (z-x)^2)^2}. \quad (22)$$

Considering all presented effects, the wavenumber of laser radiation k_0 is given as

$$k_0(z) = \frac{2\pi}{\lambda} \sqrt{\frac{p(z)}{p_a} \left(\chi_e(\lambda, \eta) + (1 - \eta)\chi_n(\lambda) \right) + 1} + \frac{z_R}{z_R^2 + (z-x)^2} \quad (23)$$

and the wavenumber of generated radiation k_q

$$k_q(z) = \frac{2\pi}{\lambda_q} \sqrt{\frac{p(z)}{p_a} \left(\chi_e(\lambda_q, \eta) + (1 - \eta)\chi_n(\lambda_q) \right) + 1} + 2\alpha I_0 z_R^2 \frac{z-x}{(z_R^2 + (z-x)^2)^2}. \quad (24)$$

Wavenumbers (23) and (24) can be substituted in the formula (13).

2.3 Medium absorption

The absorption of the generated harmonic field by the medium limits the magnitude of the signal in certain media. The absorption length L_{abs} is given as [4]

$$L_{abs} = \frac{1}{n_a \sigma} = \frac{1}{2n_a r_e \lambda f_0^2(\omega)}, \quad (25)$$

where σ is the absorption cross-section, n_a is the density of atoms, r_e classical electron radius, λ is the wavelength and f_0^2 is the imaginary part of the complex atomic scattering coefficient. The variable L_{abs} is commonly defined as the distance into a material where the beam flux has dropped to 1/e of its incident flux. If an absorption is considered during the harmonic signal propagation in the medium, the relation (15) takes a form [13]

$$E_q(L) = \sum_{j=1}^N \exp\left(-\frac{L - z_j}{2L_{abs}}\right) \exp(i \varphi_{qj}(z_j, L)). \quad (26)$$

Here we consider an average particle density to calculate L_{abs} .

2.4 Coherence length

The mismatch wavenumber Δk_q is closely related to the coherence length L_{coh} . It is the distance over which the generated harmonic radiation gets out of phase with the one generated at the beginning. The coherence length is defined as [14]

$$L_{coh} = \frac{\pi}{|\Delta k_q|} = \frac{\pi}{|qk_0 - k_q|}. \quad (27)$$

This variable will be further used to decide what medium is suitable for QPM generation.

This chapter explains the one dimensional model of the high harmonic generation on the axis along the laser beam. We need to know the evolution of the phase of both the driving and newborn radiation to define the generated field as (26). This leads to evaluating the wavenumbers (23) and (24) while considering the changes in phase due to beam propagation and dipole contribution. The next chapter describes the numerical implementation of this physical model.

3 Code implementation in MATLAB® for HHG simulations

This chapter shows the numerical implementation of the updated and improved code developed in the MATLAB® software from the work [1]. The code is based on the physical model described in chapter 2. The fundamental files are defined as classes `hhg82gf` and `sound2` that have properties and methods. The main method is function `signal` which calculates the signal of high harmonics and it also includes a function `modulation1` from class `sound2` that calculates the pressure modulation. The properties of the whole class `hhg82gf` are physical constants speed of light $c= 299792458$ m/s, permittivity of the vacuum $\epsilon_0= 8.854187817 \cdot 10^{-12}$ F/m, and the value of atmospheric pressure $p_a=101325$ Pa at temperature $T=15^\circ\text{C}$. The properties of class `sound2` are the densities of noble gases and their speed of sound, listed in table 2, and the atmospheric pressure p_a . Methods of both classes will be described in the following text. All the described codes are attached in the appendix of this work.

3.1 Pressure modulation calculation

The pressure calculation is done through the function `modulation1`. The vector of numerical values of the pressure modulation `pressureS` in the cell is the output of this method. The method `modulation1` has 7 input variables `gas`, `N`, `L`, `p`, `modulation`, `B`, and `fr`, all input variables are presumed to be in SI base units except the mean value of pressure `p` which is in bar. The speed of sound `cz` in the noble gas is set through the properties of the class according to the variable `gas`. Then the angular frequency `omega` is calculated with the frequency of the sound `fr`. After that, the wavenumber `k0` is derived from the `omega` and `cz`. The variable `modulation` switches between the types of modulations, 1 is for the homogenous medium, `sin(x)` is for the sinusoidal environment, and `step` is for the step modulation. The variables `L` and `N` are used to define the length of medium `z1` with `N` points with the length `L`. The mean value of the pressure is saved in variable `p`, it is the offset of the sine or step wave generated in the medium. The amplitude of the standing wave `B` is defined with respect to the mean value of pressure `p`, `B=1` means that the maximal value of the pressure is $p+1p=2p$ Pa and the minimum value is $p= 0$ Pa. The sine wave modulation is calculated as

$$pressureS = (p \cdot 10^5 + p \cdot 10^5 B \sin(k_0 z_1)). \quad (28)$$

If the step modulation is chosen then the numerical vector is evaluated as

$$pressureS = p \cdot 10^5 + B p \cdot 10^5 \text{sgn}(\sin(k_0 z_1)) \quad (29)$$

and values lower than the mean pressure `p` are set to 0.

3.2 Signal calculation

The signal calculation is divided into 3 functions. Firstly the Rayleigh range z_R is calculated through the input variables as

$$z_R = \frac{\lambda}{\pi \arctan\left(\frac{1}{2F}\right)}, \quad (30)$$

where the `lambda` is the wavelength and `F` is the F-number defined as

$$F = \frac{f_c}{d} \quad (31)$$

with the focal length of the focusing element `f_c` and the diameter of the beam on the element `d`. After the Rayleigh range z_R is evaluated it is used as an input variable for the function that calculates the dipole addition to the high harmonics wavenumber according to (22) with the same input variables. The intensity I_0 is preset to the value $I_0 = 2 \cdot 10^{18} \text{ W/m}^2$ and the proportional constant is set to $\alpha = 10^{-18} \text{ m}^2/\text{W}$.

The core function `signal` calculating the intensity I_{out} over the distance in a cell z is written in the method `signal`. This function has 14 input variables, most of which are used in the functions described above. The following steps are performed:

1. Defining the length vector z with N points and distance of the cell L , defining classes `sound2` and `MedClass`, defining the high harmonic wavelength $\lambda_q = \lambda/q$, and creating empty variables to allocate memory for them
2. Calculating the pressure modulation with the input variables `gas`, N , L , p , `modulation`, `A`, `fr`
3. Evaluating the susceptibilities of the neutrals and plasma for given `gas` for both driver field λ and λ_q with `eta`
4. Evaluating the integrands of laser radiation f and high harmonic radiation g as (23) and (24)
5. Integrating the integrands f , g from the last step with cumulative trapezoidal integration³ and evaluating the average absorption length `atlaverage` for the radiation λ_q
6. Defining the phase ϕ with the calculated integrals f_p and g_p from the last step according to (13) and defining the signal field E_q according to (26)
7. Calculating auxiliary variable `pom0` to determine the field E_q and intensity $I_{\text{out}} = |E_q|^2$ accumulated in each point of z

Class `MedClass` is taken from the work [16]. The properties of this class are important physical constants in regular circumstances. The methods of this class are the functions to evaluate the susceptibility of neutral gas for the laser field `sDriver`, the susceptibility of neutral gas for the generated field `sXuv`, the susceptibility of plasma `sPlasma`, and the function to calculate the absorption length `aLength` from equation (25). The overall scheme of the implemented code is seen in figure 4.

³Numerical approximation of definite integral [15]

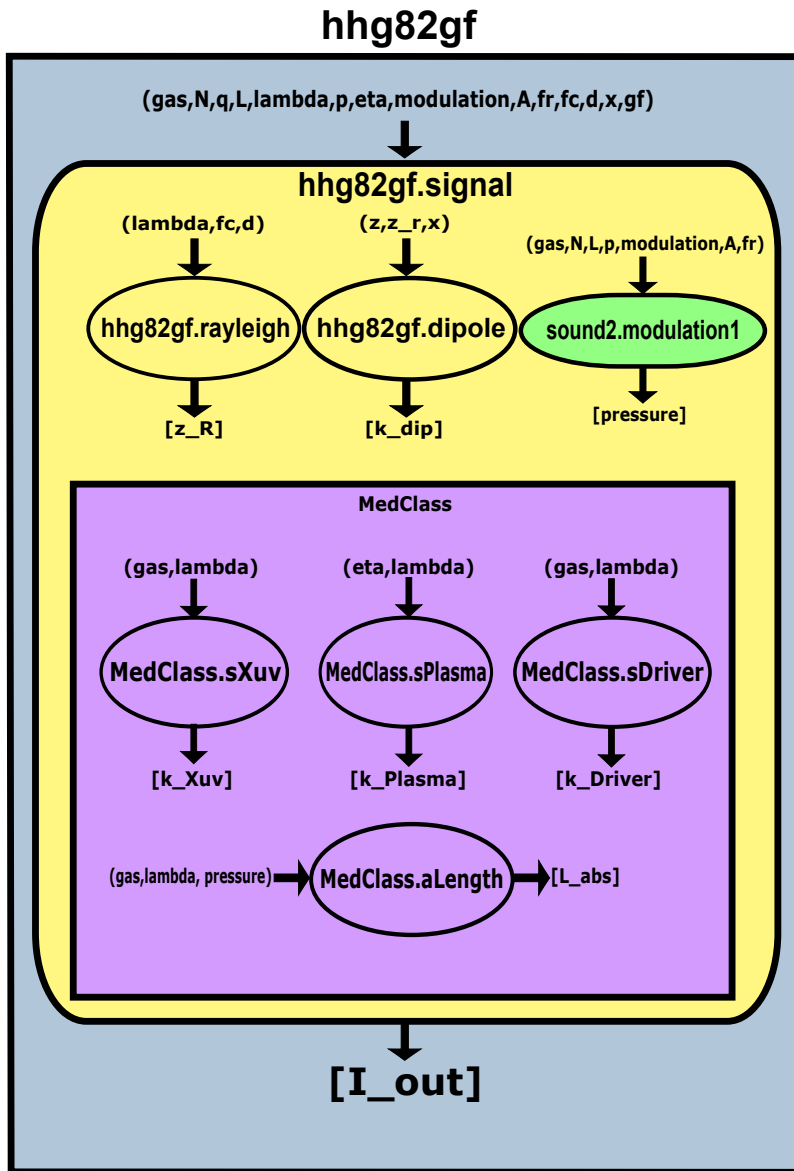


Figure 4: The scheme of the implemented code calculating intensity I_{out} over the distance z

3.3 Analysis of phase and wavenumber

In the next chapter, it will be useful to know the change of phase of the radiation in space in order to be able to design the geometry of the medium that will be suitable for single high-harmonic generation. We shall describe the evolution of both laser and high harmonics radiation with the mismatch vector (3). The ideal PM condition is $\Delta k_q = 0$. There is no need to write a function that calculates this variable since the wavenumbers k_0 and k_q are both computed during the evaluation of the intensity in the cell. Nevertheless, the information contained in this relationship between these two fields is crucial for understanding the QPM. Our point of interest will be the integral of the mismatch vector

$$\varphi_{\Delta k_q} = \int_0^L \Delta k_q dz \quad (32)$$

and the change of such phase and wavenumber per one period of the density modulation

$$\Lambda = \frac{c_s}{f_s}, \quad (33)$$

where c_s is the speed of sound in the given noble gas and f_s is the frequency of the standing wave in the medium.

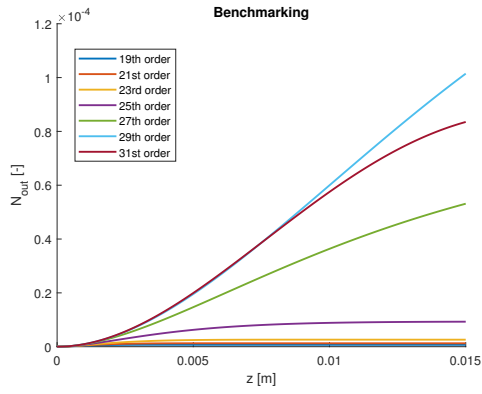
3.4 Benchmarking

In order to verify that the code works properly, we shall take a look at the benchmarking of it with an analytical model of HHG in homogeneous media developed in paper [13]. Formula (1) is used

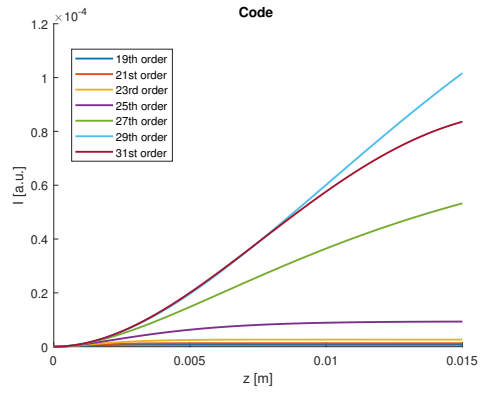
$$N_{out} = \rho^2 A_q^2 \frac{4L_{abs}^2}{1 + 4\pi^2 \left(\frac{L_{abs}^2}{L_{coh}^2}\right)} \left(1 + \exp\left(-\frac{L_{med}}{L_{abs}}\right) - 2 \cos\left(\frac{\pi L_{med}}{L_{coh}}\right) \exp\left(-\frac{L_{med}}{2L_{abs}}\right) \right) \quad (34)$$

from the article, where L_{med} is the length of the medium, L_{abs} is the absorption length, and L_{coh} is the coherence length. The gas density ρ and amplitude of atomic response A_q at the frequency ω_q were set to 1 since we do not consider them in our code. The number of emitted photons N_{out} is then proportional to the absorption, coherence, and medium length. Those lengths are derived from the calculations in the code and used in equation (34) afterward.

The code itself has 13 input parameters such as the noble gas that is used *gas*, the number of points in space N , or the length of the medium L . However, the deciding variables for the calculation of the signal in the homogeneous gas cell are the mean value of pressure p , the percentage of the ionized particles in the cell η , and the wavelength λ . We are able to evaluate the absorption length $L_{abs} = L_{abs}(gas, \lambda, p)$ and coherence length $L_{coh} = L_{coh}(gas, \lambda, p, \eta)$ from those 3 variables. A case in argon where the parameters were set $\lambda = 810$ nm, $p = 30$ mbar, $\eta = 4.5\%$ is seen in figure 5. As follows from this figure, the code reproduces the results of the analytical model very well. Therefore the code is working properly in a homogeneous medium from the numerical point of view since the values for the signal calculated by the code and equation (34) are the same.



(a) The number of emitted photons N_{out} in each point of gas cell z



(b) The signal I in each point of the gas cell z

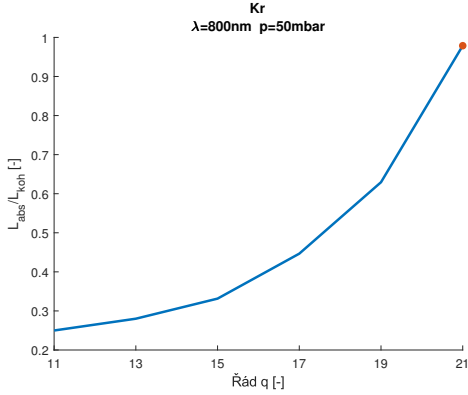
Figure 5: Comparison of code and the article [13], the graph on left is calculated by equation (34) and the graph on the right is calculated by the developed code

4 Optimizationalization of single harmonic frequency generation

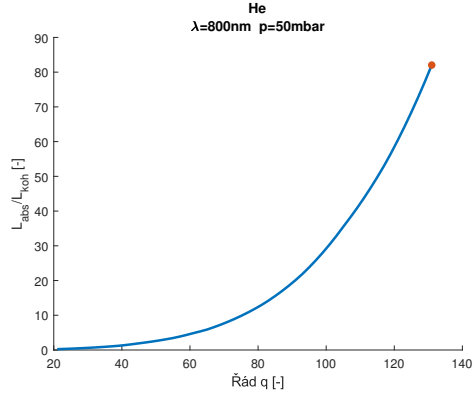
In this section, we focus on the key input variables that fundamentally change the output harmonic. We aim for the best set of parameters for selective filtering of a single harmonic order that is generated in a periodically modulated medium. The key variables are mainly the geometrical wavenumber k_g , the mean value of pressure in the cell p , and the frequency of the modulation fr . We will see graphs of η over k_g and we shall examine this more closely in the following text. We focus on ionization η because it is controlled by the configuration of the laser pulse that is used in the process.

4.1 Ratio of absorption and coherence length

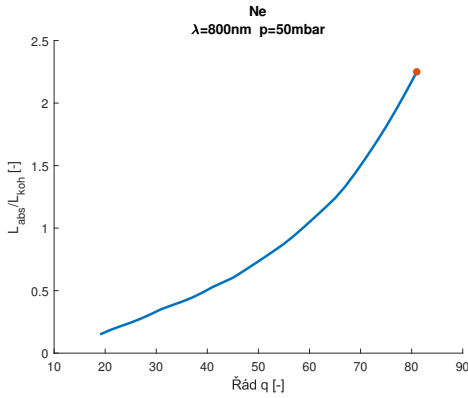
One of the good indicators that the circumstances are right for filtration is the ratio of absorption and coherence length L_{abs}, L_{coh} . The absorption length L_{abs} and coherence length L_{coh} were described in chapters 2.3 and 2.4 and calculated as (25) and (27). The goal is to maximize the ratio $\frac{L_{abs}}{L_{coh}}$ which tells us the radiation is not strongly absorbed. The ratio will depend on the choice of noble gas, we can see the ratios for krypton, helium, neon, xenon, and argon in figures 6a to 6e. The graphs are plotted for the mean value of pressure $p = 50$ mbar in the homogeneous gas, wavelength of the laser $\lambda = 800$ nm and wavenumbers k_0 and k_g are calculated as (23) and (24). We can see from these graphs that helium and argon have high ratios of $\frac{L_{abs}}{L_{coh}}$ and thus they are the best choices for QPM generation. Note that the maximum order considered here is the cutoff order for the intensity at which the laser field reaches suppression of the Coulomb barrier of the atom. Both L_{coh} and L_{abs} are linearly proportional to density, so their ratio should be density independent.



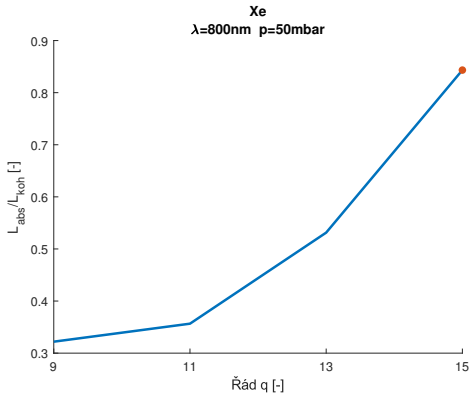
(a) Graph of the dependence $\frac{L_{abs}}{L_{koh}}$ over the order of high harmonic q in krypton



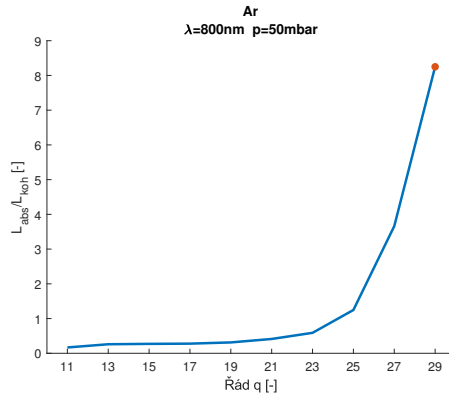
(b) Graph of the dependence $\frac{L_{abs}}{L_{koh}}$ over the order of high harmonic q in helium



(c) Graph of the dependence $\frac{L_{abs}}{L_{koh}}$ over the order of high harmonic q in neon



(d) Graph of the dependence $\frac{L_{abs}}{L_{koh}}$ over the order of high harmonic q in xenon



(e) Graph of the dependence $\frac{L_{abs}}{L_{koh}}$ over the order of high harmonic q in argon

Figure 6: Ratios of absorption and coherence length L_{abs} and L_{koh} in noble gases over the order q , the red dot in graphs symbols the cut-off order

4.2 Phase evolution during propagation in the cell

The main idea behind quasi-phase-matching in a density-modulated medium is to create local circumstances in the gas cell to gain a stronger signal when phase-matching is not achieved. If the PM condition is not met, the signal oscillates without amplification. The use of density modulation creates spots in the medium where the PM is met and a signal is amplified. An example of achieved QPM for 29th order in argon is seen in figure 7. This example clearly shows that QPM is a way to realize selective filtering. The selective filtering of single harmonic order is achieved solely by density modulation. The important aspect during selective filtering in the gas cell is the evolution of the mismatch wavenumber k_q .

If the phase is calculated as (12), for each harmonic order a rule for fulfilling selective filtering using QPM appears. The phase needs to stay constant in the first half of the medium period and then gain 2π in the second half of the period. That is an ideal case but in most cases, the phase in the first half is not constant and gains value from 0 to π . This specific evolution of the phase may be fulfilled only by the change of the geometric phase of the original radiation. The evolution of the phase ϕ of the mismatch wavenumber Δk_q of the order 29 from figure 7 is plotted in figure 8. We can see that the phase gained in the first half of the medium is not higher than π and it is equal to 2π at the end of the period. Figure 9 shows the evolution of phase ϕ for order 23 from figure 7 where the condition mentioned before is not met and the signal is lower than the one of order 29. This naturally leads to the interest in the geometrical phase of the laser beam.

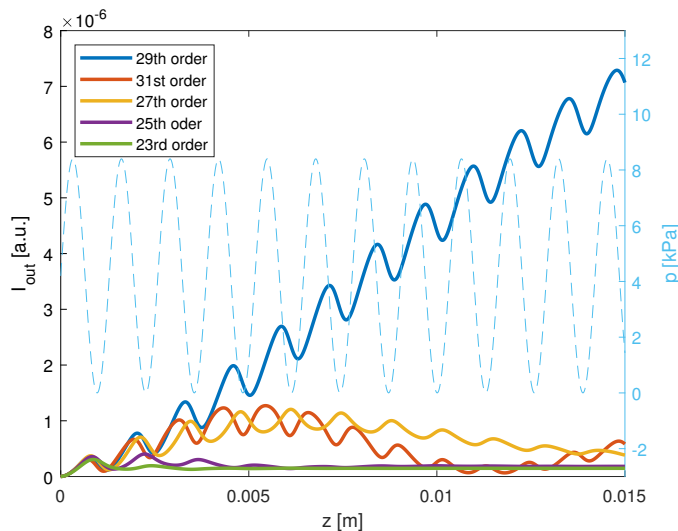


Figure 7: An example of single high harmonic order generated with QPM in argon

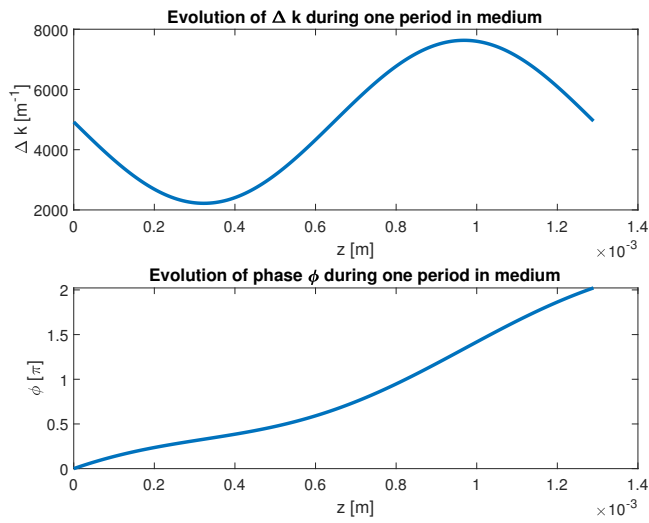


Figure 8: The evolution of phase ϕ of mismatch wavenumber Δk_q during one period of the medium of order 29 from graph 7

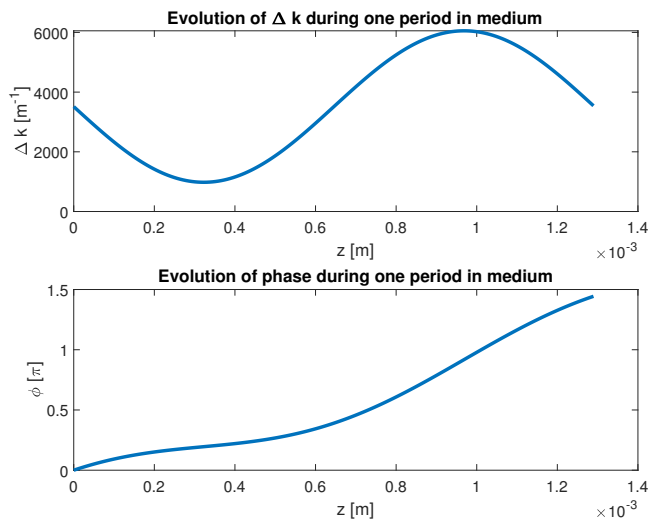


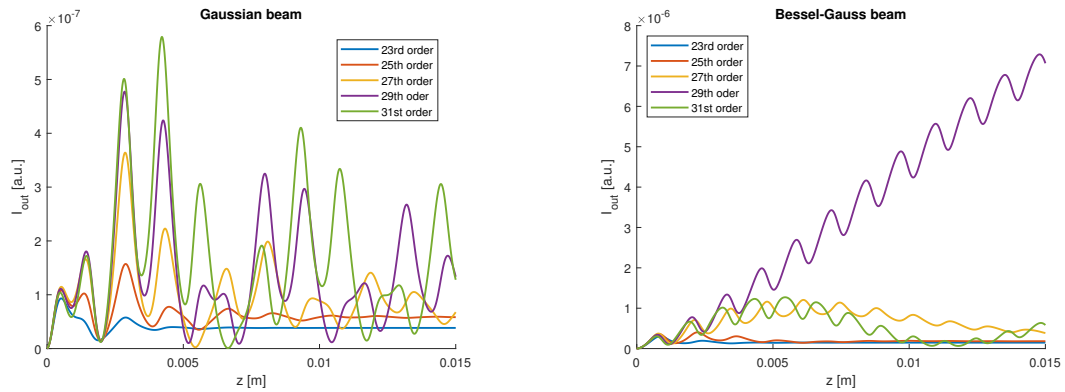
Figure 9: The evolution of phase ϕ of mismatch wavenumber Δk_q during one period of the medium of order 23 from graph 7

4.3 Geometrical dispersion segment of k_0

We saw in equation (23) that the Gaussian beam brings in the geometrical dispersion in the form of

$$k_g = \frac{z_R}{z_R^2 + (z - x)^2}, \quad (35)$$

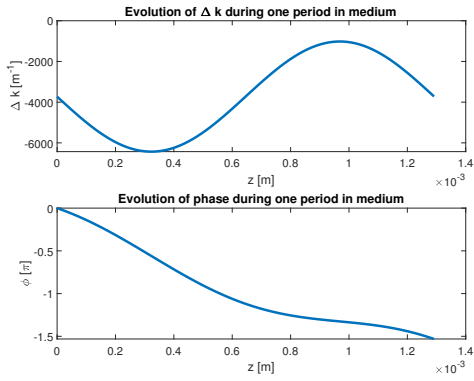
so the addition to the wavenumber k_0 depends on the axis coordinate z . The example of single HH order filtered by a density modulation in chapter 4.2 was not shown on the Gaussian beam but the Bessel-Gauss beam was used instead. We can see the comparison of the signals for orders 23 to 31 for the Gaussian and Bessel-Gauss beams in figure 10. If we take a look at the progression of mismatch wavenumber Δk and its phase ϕ for order 29, figure 11, we clearly see that the Gaussian beam does not achieve quasi-phase-matching. The Bessel-Gauss beam had set a constant k_g and the phase changed by 2π at the end of the period. Hence the BG beam is a better choice for QPM selective filtering.



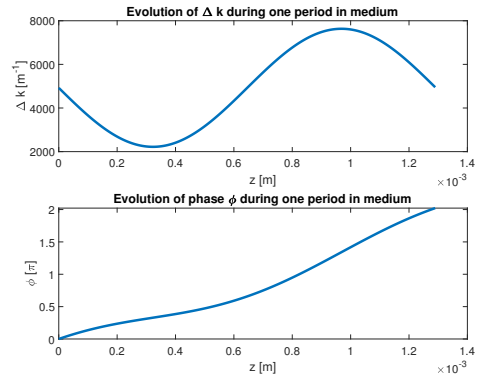
(a) The evolution of signal over distance for order 23 to 31 while using Gaussian beam

(b) The evolution of signal over distance for order 23 to 31 while using Bessel-Gauss beam

Figure 10: Comparison of the Gaussian and Bessel-Gauss beam for selective filtering



(a) The evolution of mismatch wavenumber and phase over one medium period for Gaussian beam



(b) The evolution of mismatch wavenumber and phase over one medium period for Bessel-Gauss beam

Figure 11: The mismatch wavenumber and phase evolution for Gaussian and Bessel-Gauss beam for order 29

4.4 Ionization η dependence over k_g for sinusoidal modulation

Ionization η of the gas is another variable closely related to the settings of the laser system since it corresponds to the laser intensity both in time and space. We saw that the geometrical segment of the wavenumber k_g significantly changes the output of the generation. The ionization η has the same significance because every order has an optimal amount of ionization to achieve PM. To analyze the situation when we try to accomplish QPM, the code was used to plot 3D graphs where on the x-axis is the geometrical wavenumber of the laser radiation k_g , on the y-axis is the ionization of the gas η , and on the z-axis is the maximum magnitude of the signal in the cell. An example of this colormap for order 29 in argon with sinusoidal density modulation with the period $\Lambda = 1.29$ mm, the amplitude of sinus wave $A = 1$, the mean value of the pressure $p = 42$ mbar, and the wavelength of the laser $\lambda = 800$ nm is seen in figure 12. The amplitude $A = 1$ means that the maximal amplitude of the wave is 100% from the mean value of pressure p . The most bright line in the graph in the bottom left corner corresponds to the region where the phase-matching is fulfilled, we know that because we can calculate the optimal values for ionization η , shown in table 1. Alternatively, we could plot the colormap for a case with no pressure modulation and see that the only region present is the one with PM. The other two interrupted lines correspond to the quasi-phase-matching and higher-order phase quasi-phase-matching. The higher-order phase matching changes at the end of the period of the modulated medium by 4π .

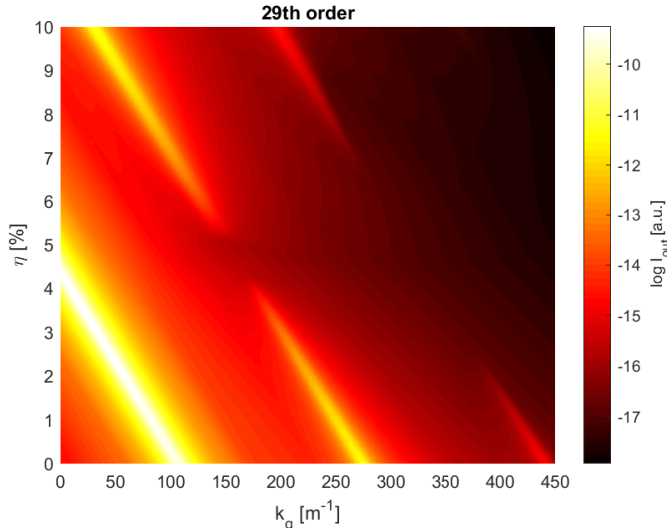


Figure 12: The colormap of ionization η over geometrical wavenumber k_g with the maximal strength of the signal in the cell for the 29th order with the logarithmic scale of the intensity

Retrospectively, the colormaps can serve as a manual to find a good set of parameters to achieve QPM for specific order. If we ionize the gas to the value of $\eta = 9.7\%$ and create a beam that has geometrical wavenumber $k_g = 36.36 \text{ m}^{-1}$ the signal evolves as in figure 13.

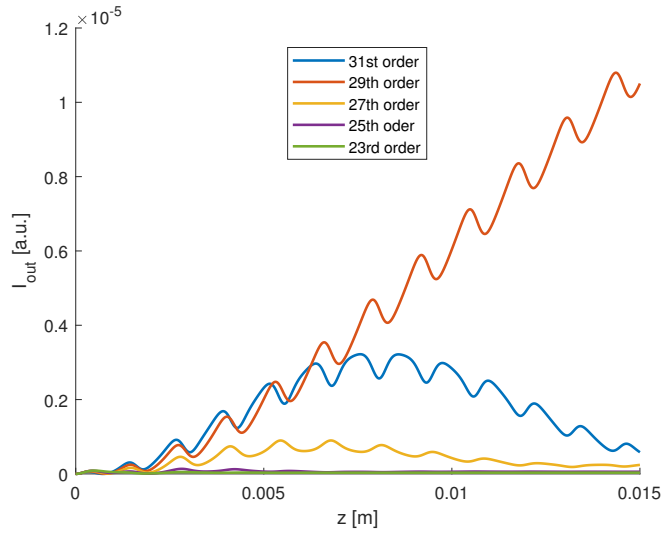


Figure 13: Signal evolution for the ionization $\eta = 9.7\%$ and $k_g = 36.36 \text{ m}^{-1}$ that was acquired from the colormap 12

Same colormaps were created for the same set of parameters as for the order 29. Figure 14 shows main lines for single orders in the phase-matching and quasi-phase-matching region. These lines were linearly interpolated from the colormaps for each order.

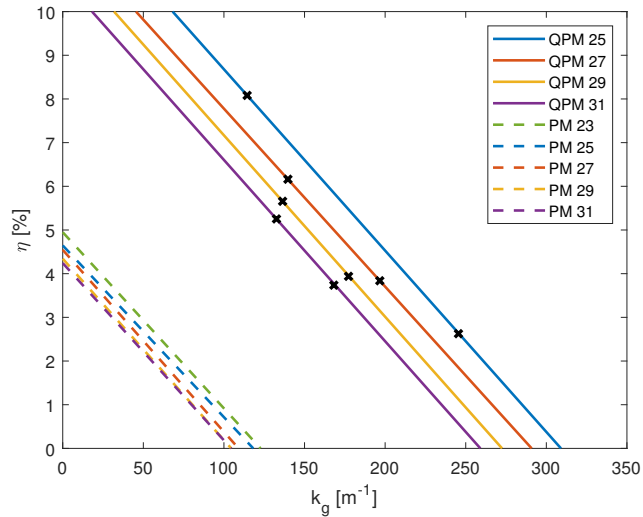


Figure 14: Phase-matching and quasi-phase-matching lines interpolated from colormaps

We shall investigate how the colormap will change in the case of step pressure modulation. The input parameters are the same as for the sinusoidal modulation for order 29 in argon - $fr = 247 \text{ kHz}$, $A = 1$, $p = 42 \text{ mbar}$, $\lambda = 800 \text{ nm}$. The comparison of the sinusoidal and step modulation is presented in figure 15.

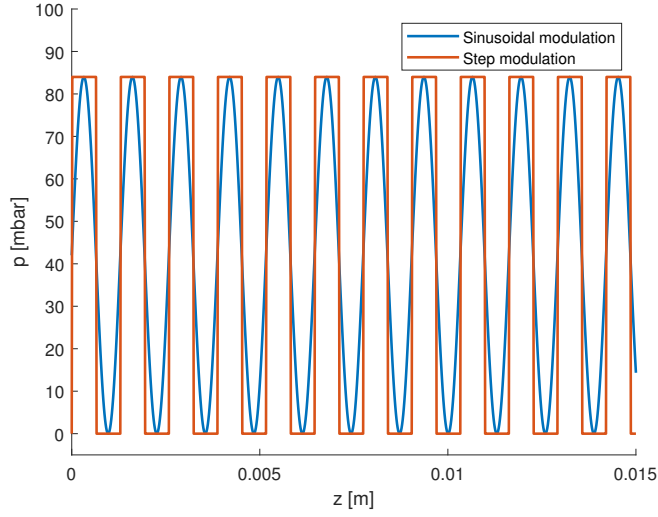


Figure 15: The comparison of sinusoidal and step pressure modulation, the vertical axis show pressure p and horizontal axis the distance in the gas cell z

The colormap for the step pressure modulation is showed in figure 16. This colormap and the one with the sinusoidal modulation, figure 12, looks alike but the main difference is the region with higher QPM in the top right corner of the colormap. There is also the same singularity in the form of discontinuity in the middle of the quasi-phase-matching line as in the previous modulation. The signal evolution of orders 23 to 31 in point $k_g = 163.63 \text{ m}^{-1}$, $\eta = 4.6\%$ is shown in figure 17.

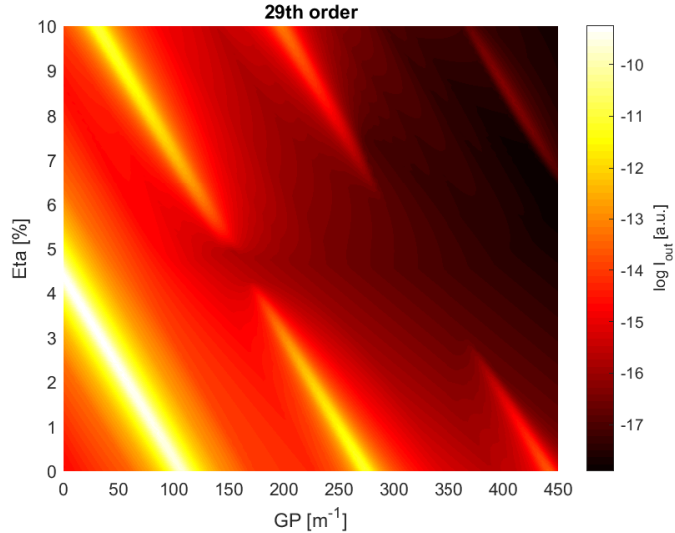


Figure 16: The colormap of ionization η over geometrical wavenumber k_g with the maximal strength of the signal in the cell for the 29th order with step pressure modulation in argon

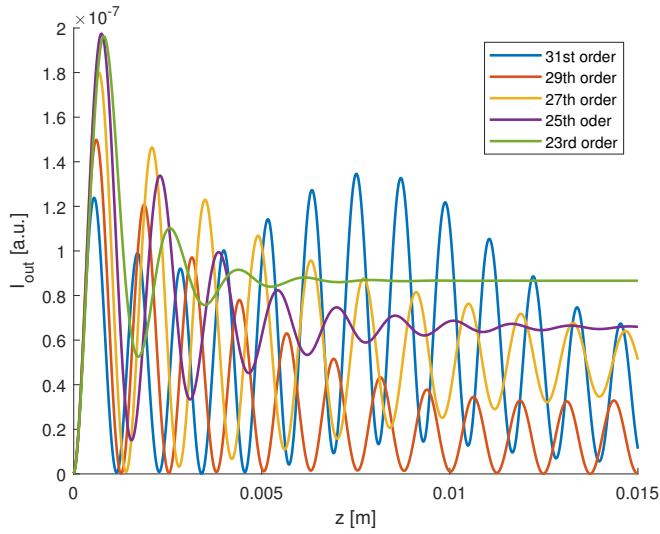
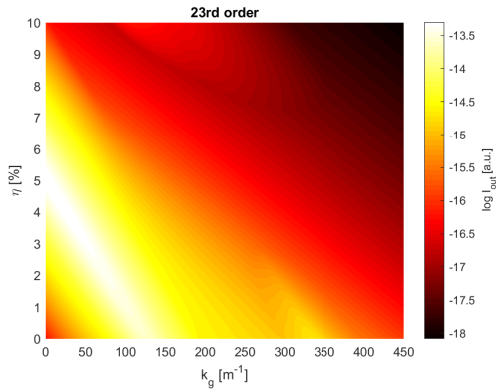


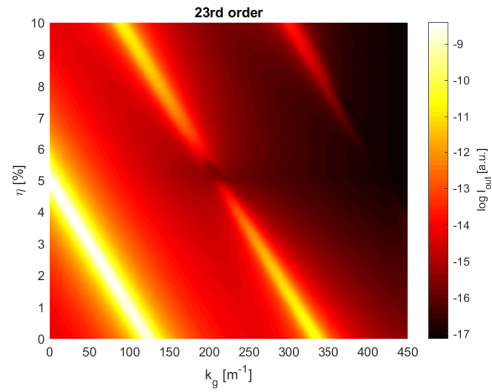
Figure 17: The signal evolution for orders 23, 25, 27, 29, and 31 for the point $k_g = 163.63 \text{ m}^{-1}$, $\eta = 4.6\%$ in the singularity region for step modulation

4.5 Absorption effect for HHG

As we have seen in figure 6, the absorption effect is important for the generation. Figure 14 misses the QPM line for the 23rd order. That is because the absorption in the gas is strong for this order in comparison with others and the newborn high harmonic field is almost completely suppressed. We neglect the absorption effect and define the generated high harmonic field as (15). The comparison of colormaps with neglected absorption for 23rd order with the same input parameters as in section 4.4 for step modulation is shown in figure 18. Therefore, the lower orders may not be eligible for selective filtering because of the absorption effect.



(a) With absorption



(b) Without absorption

Figure 18: The comparison of colormaps of ionization η over wavenumber k_g for 23rd order with absorption and neglected absorption in the gas

4.6 Monochromaticity of QPM

Figure 14 shows that quasi-phase-matching regions are close to each other. We were focused on the main lines of QPM areas but there is no information about the spread or if the adjacent orders overlap each other. For such reason, we can look at the colormap with the signal of specific order divided by the sum of the adjacent ones, in the example of 29th order

$$\frac{I_{out}^{(29)}}{I_{out}^{(27)} + I_{out}^{(31)}}. \quad (36)$$

Given example (36) is presented in figure 19. Those values of k_g and η are not the ones with the biggest power of signal but they are the most suitable for selective filtering of the 29th order. It also shows that selective filtering can not be achieved in the PM region.

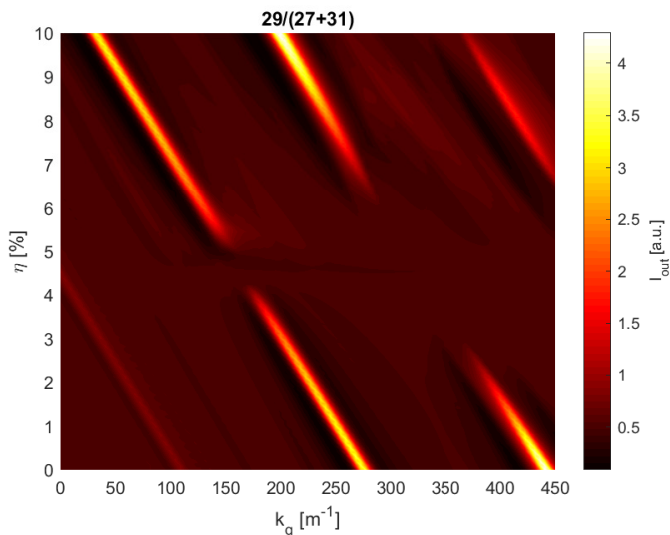


Figure 19: The colormap of monochromaticity for 29th order

This colormap is also indicator how precise the experimental setup would need to be if we tried to achieve selective monochromatic generation of this harmonic order because it gives the ranges of ionization η and wavenumber k_g for QPM.

The colormaps show that in order to achieve the selective filtering during the generation, the input parameters need to be set for quasi-phase-matching. Selective filtering can not be accomplished in the phase-matching region. The deciding factor for using QPM as a tool for the filtering is the change of phase of the laser beam during one period of the modulated medium. For this reason, the Gaussian beam is not eligible for the filtering because the change of phase during the one period is too small. The alternative is the Bessel-Gaussian beam.

5 Pulse design for QPM in density modulated target

The ultrashort laser pulse inevitably ionizes the noble gas during the HHG. The degree of ionization increases from $\eta = 0\%$ as the intensity of the pulse grows in time. The change of geometric phase with the ionization is crucial for selective filtering. For this reason, this section connects the results of the implemented 1D code with the theory of ionization in order to design a pulse suitable for selective filtering in a density-modulated target. A laser beam with a pulse is designed based on the results of the simulations. We saw (Fig. 14 and 16) that high harmonics have linear dependence of ionization η of gas over the geometrical wavenumber k_g if the maximal signal is to be achieved. Therefore, a laser pulse is designed with properties allowing such optimal generation in the quasi-phase-matching region. Each value of k_g has the corresponding value of η and the pulse need to follow this dependence in time t . By knowing the evolution of the geometrical wavenumber in time $k_g(t)$, the radius r in time t of the Bessel-Gaussian beam is calculated. Finally, an optical setup with suitable parameters for the filtering using optimal QPM for a single harmonic order is proposed.

5.1 Ionization by an optical pulse

The infinitesimally small ionization probability $d\eta$ of the atom in a time domain is given as

$$d\eta = (1 - \eta)w(t) dt, \quad (37)$$

where $w(t)$ is the ionization rate. We receive the solution of this differential equation in the form of

$$\eta(t) = 1 - \exp\left(-\int_{-\infty}^t w(t') dt'\right). \quad (38)$$

Since we consider ionization by an optical field the ionization rate function $w(t)$ will depend on the driving laser pulse shape. The approximation of the ionization rate for complex atoms in an alternating electromagnetic field is described by the ADK model [17]

$$w_{ADK}(t) = C_{n^*l}^2 f(l,m) I_p \left(\frac{3E(t)}{\pi(2I_p)^{\frac{3}{2}}}\right)^{\frac{1}{2}} \left(\frac{2(2I_p)^{\frac{3}{2}}}{E(t)}\right)^{2n^* - |m| - 1} \exp\left(-\frac{2(2I_p)^{\frac{3}{2}}}{3E(t)}\right), \quad (39)$$

where I_p is the ionization energy and $E(t)$ is the driving electromagnetic field. Equation (39) is derived for the system of atomic units, $\hbar = m_e = e = 1$ and the coefficients are defined as

$$C_{n^*l} = \left(\frac{2e}{n^*}\right)^{n^*} (2\pi n^*)^{-\frac{1}{2}} \quad (40)$$

and

$$f(l,m) = \frac{(2l+1)(l+|m|)!}{2^{|m|}|m|!(l-|m|)!}, \quad (41)$$

where $n^* = \frac{Z}{\sqrt{2I_p}}$ is the effective principal quantum number with the charge of the atomic residue Z , l is the azimuthal quantum number, and m is the magnetic quantum

number. The ADK model (39) was further examined and corrected in [18]. The code that calculates the ionization probability was developed by Jan Vábek at ELI [19]. An example of the output of the code is presented in figure 20. The solid blue line describes the dependence of ionization probability η over time t while the orange dashed line shows the evolution of electric field amplitude of the Gaussian pulse E over time t . The field envelope of the Gaussian pulse has a form

$$E(t) = E_0 \exp\left(-\frac{2 \log(2)t^2}{\tau^2}\right). \quad (42)$$

The graph was simulated for the central wavelength $\lambda = 800$ nm in argon, with the peak intensity of the pulse $I_0 = 1.785 \cdot 10^{14}$ W/cm², and the pulse duration⁴ $\tau = 40$ fs. The amplitude of electric field E_0 is derived from the formula [20]

$$I_0 = \frac{1}{2} \varepsilon_0 c E_0^2. \quad (43)$$

We can see that the ionization has the biggest increase when the pulse is reaching its peak value and after that, the ionization remains constant.

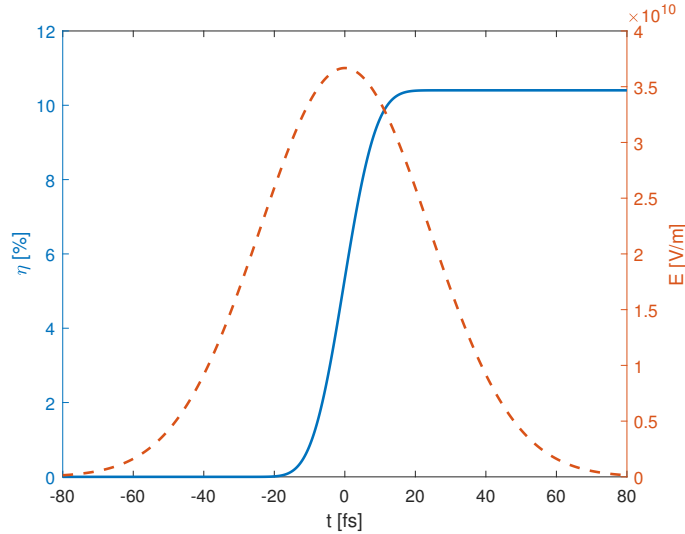


Figure 20: The ionization η dependence over time t , dashed orange line for the Gaussian pulse, solid blue line calculated by the corrected ADK formula model

⁴Defined as the full width at half maximum of the intensity

5.2 Dependence of k_g over time t

Example 20 showed us the behavior of ionization probability η in time t . Since we know the values of η and k_g for the best signal generated in the QPM region from the colormap, we can get the required dependence of k_g over time t . This can be done by associating value k_g for time t because we know the dependence $\eta(t)$ from the ADK model, we receive $k_g(\eta(t))$. The calculated dependence $k_g(\eta)$ from the code does not contain any information about the time direction. The pulse may follow the dependence $k_g(\eta)$ from the highest or the lowest value of η in time. That said, we ionize the gas with the laser pulse with the assumption of growing degree of ionization and we have to consider η changing with time from the lowest value of η . This gives us the evolution $k_g(t)$. An example of k_g over t is shown in figure 21. The blue line is the ionization probability from figure 20 and the orange line shows the evolution of k_g . It is k_g as for high harmonic order from figure 12. The dependence of k_g on time t is almost linear and it will be used in the following text to determine the spatio-temporal structure of the BG pulse.

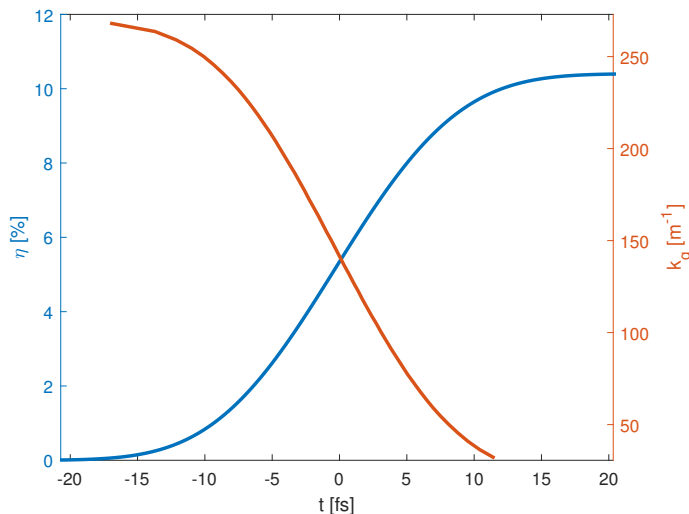


Figure 21: The dependence of ionization degree η and geometrical phase k_g over time t for the QPM of the 29th order

5.3 Beam design

We can calculate the divergence $\theta(t)$ of the beam in the focus by the relation

$$\theta(t) = \arccos \left(1 - \frac{k_g(t)}{k} \right), \quad (44)$$

where k is the wavenumber of a plane wave. This is based on the consideration schemed in figure 22. The projection k_g of the k vector is taken on the longitudinal axis of the beam and it is related to the k vector of the plane wave.

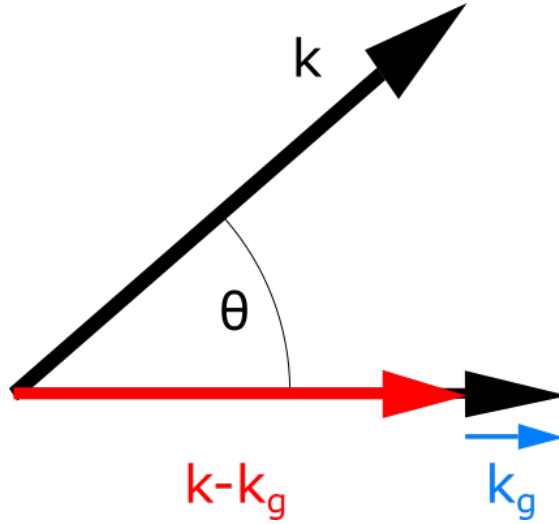


Figure 22: Scheme of wave vectors in the focus of the beam

With the addition of the focal length of the focusing element f , we are able to calculate the radius of the beam $r(t)$ on the focusing element as

$$r(t) = f \tan \theta(t). \quad (45)$$

A graph of radius r over time t calculated with the focal length $f = 2$ m for the evolution of $k_g(t)$ from figure 21 is presented in figure 23. The beam is hollow and the time window in which the radius needs to change is $\Delta T \doteq 29$ fs.

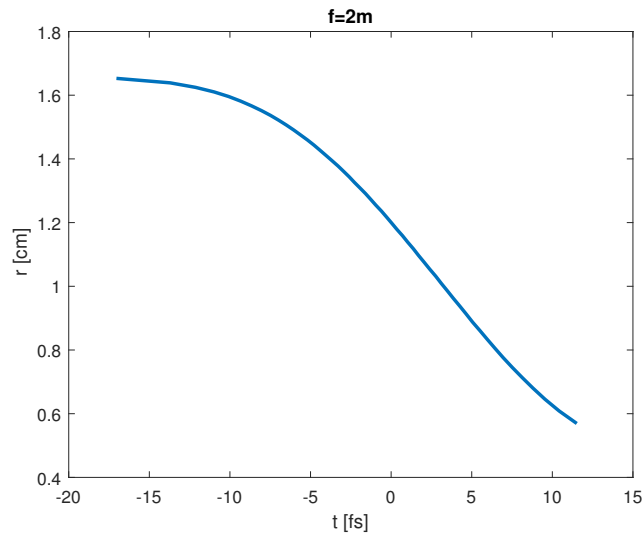


Figure 23: The dependence of effective radius of the BG beam r over time t

5.4 Optical setup

One of the ways to generate the time delay for arriving light in the focus is to use a spherical singlet lens. The path of the light differs for different radii on the lens and this induces a time delay in the focus. The time delay between the arrival of the beam on the rim of the lens r_0 and r from the center of the lens in the focus can be evaluated on singlet lens as [21]

$$\Delta T(r) = \frac{r_0^2 - r^2}{2c} \left(\frac{1}{R_1} - \frac{1}{R_2} \right) \left(\lambda \frac{dn}{d\lambda} \right) = \frac{r_0^2 - r^2}{2c} \lambda \frac{d}{d\lambda} \left(\frac{1}{f} \right). \quad (46)$$

The focal length f is associated with the refractive index n and the radii of curvatures R_1 and R_2 as

$$\frac{1}{f} = (n - 1) \left(\frac{1}{R_1} - \frac{1}{R_2} \right). \quad (47)$$

The difference of the radii can be expressed as

$$\left(\frac{1}{R_1} - \frac{1}{R_2} \right) = \frac{1}{f(n - 1)} \quad (48)$$

from equation (47) and by substituting this difference in equation (46) we receive

$$\begin{aligned} \Delta T(r) &= \frac{r_0^2 - r^2}{2c} \lambda \frac{d}{d\lambda} \left(\frac{1}{f} \right) \\ &= -\frac{r_0^2 - r^2}{2cf(n - 1)} \left(\lambda \frac{dn}{d\lambda} \right). \end{aligned} \quad (49)$$

If we know the refractive index n and its change with the wavelength $dn/d\lambda$ of the material of the lens, we can calculate the time difference ΔT . In the example of the hollow Bessel-Gauss beam of Ti:Sapphire $\lambda = 800$ nm being focused by the LASF9 lens with the focal length $f = 2$ m, refractive index $n_{LASF} = 1.8325$ and chromatic dispersion $dn/d\lambda = -0.0524 \mu\text{m}^{-1}$ [11], the time delay for the radii $r_0 = 1.65$ cm and $r = 0.57$ cm from the figure 23 is $\Delta T \doteq 10$ fs. This is clearly not enough since we need $\Delta T = 29$ for our example and different material would be needed or the focal length f would have to be adjusted. Such material may not exist and we need an alternative way to generate a longer time delay in the focus between the ray coming from the rim and the radius r . One way is to create an optical setup made of multiple singlet lenses, as demonstrated in figure 24.

Chapter 5 focuses on the pulse and beam design for selective filtering using quasi-phase-matching of a single order. The colormaps from the code simulations contain the dependence of the ionization η over the wavenumber k_g of the laser radiation. The evolution of k_g in time t is derived from the ionization ADK model and colormap. The evolution of the wavenumber $k_g(t)$ is converted to the beam divergence $\theta(t)$. A beam radius r is calculated for the derived divergence θ and lens with the focal length f . Finally, an optical setup is proposed for the required spatio-temporal coupling of the pulse which can be represented by a dependence of the effective radius of the BG beam on time change of radius in time $r(t)$ in order to achieve selective filtering using QPM.

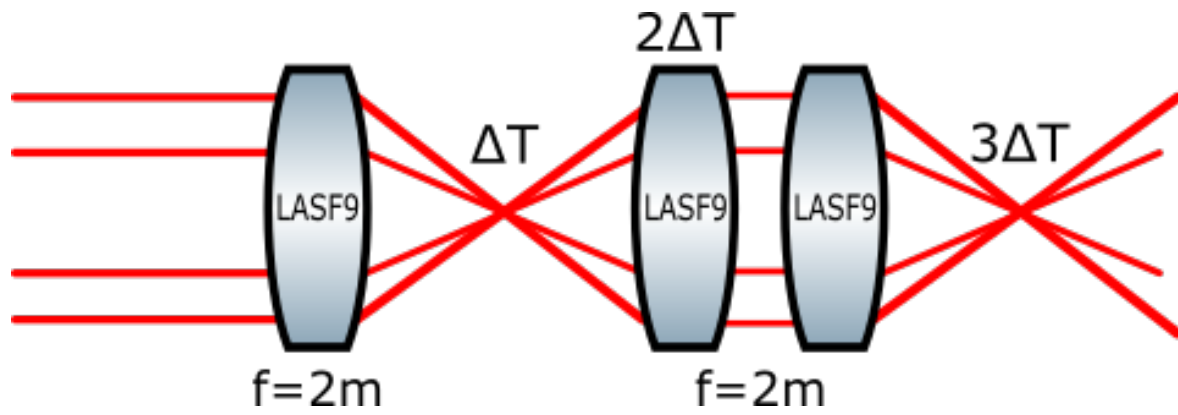


Figure 24: Optical setup for the hollow beam and achieving delay ΔT

6 Density modulated gas targets

This chapter focuses on the possible implementations of the gas targets suitable for density modulation. Two methods of modulating density in the gas cell are presented. The first one is by the standing acoustic wave and the second one is by the series of gas jets. The following subchapters describe those methods in more detail.

6.1 Standing acoustic wave

The standing acoustic wave⁵ can be generated by two piezo-ceramic rings facing each other. If the rings oscillate with the same frequency, the standing wave will be formed between the rings on the longitudinal axis. For acoustic target design, an experiment was conducted with such rings with the goal of generating standing acoustic wave. Firstly, the resonant frequency of the rings was measured on air. This was done by connecting the first piezo ring to the signal generator with an amplifier as an emitter and connecting the second ring to the oscilloscope as a receiver while facing each other on the same level. The resonance curve is plotted in figure 25 where it is clear that the optimal sound frequency for generation is $\nu_{res} = 267$ kHz.

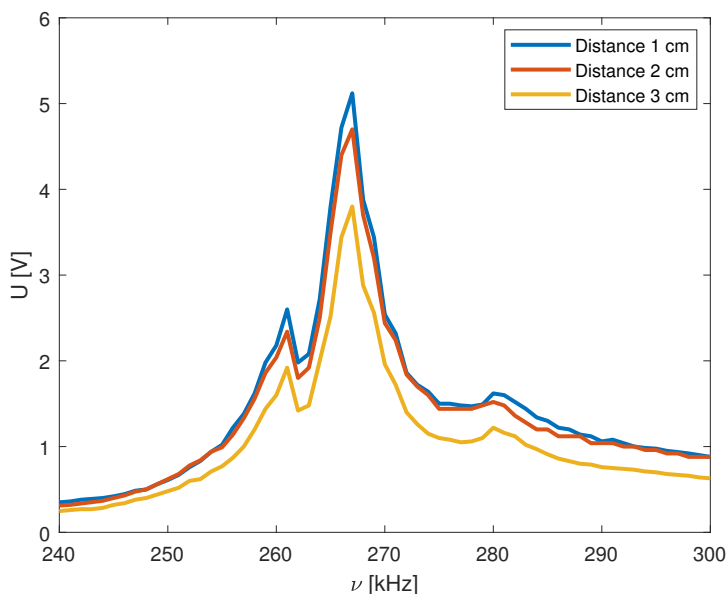


Figure 25: Resonance curve of piezo-ceramic rings, voltage U was measured on the oscilloscope for the frequency of the sinus sound wave ν

Afterward, the piezo elements were connected in parallel to the signal generator with an amplifier and the signal frequency was set to $\nu_{res} = 267$ kHz. The rings were placed in 3D-printed holders with the distance $d = 1.6$ cm between them. The standing wave was measured by a multi-pass of laser diode pulse with the propagation direction

⁵Described in more detail in [1], [22], [23]

perpendicular to the axis of the rings. A phase map from a waveform detector was captured, figure 26. The phase map shows the formation of the standing wave with the frequency calculated according to (33) as $fr = 343/267 \cdot 10^3 = 1.3$ mm.

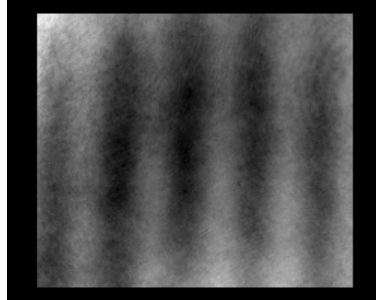


Figure 26: Phase map captured from the wavefront sensor

The first acoustic experiment confirmed that piezo-ceramic rings are able to produce standing wave on air. A more sophisticated acoustic target design was created for a density-modulated high harmonic generation. This design is shown in figure 27. Two piezo elements with attached conical surfaces facing each other produce a standing wave on the axis of the laser beam. The gas cell is filled with the noble gas and the whole cell is placed in a vacuum.

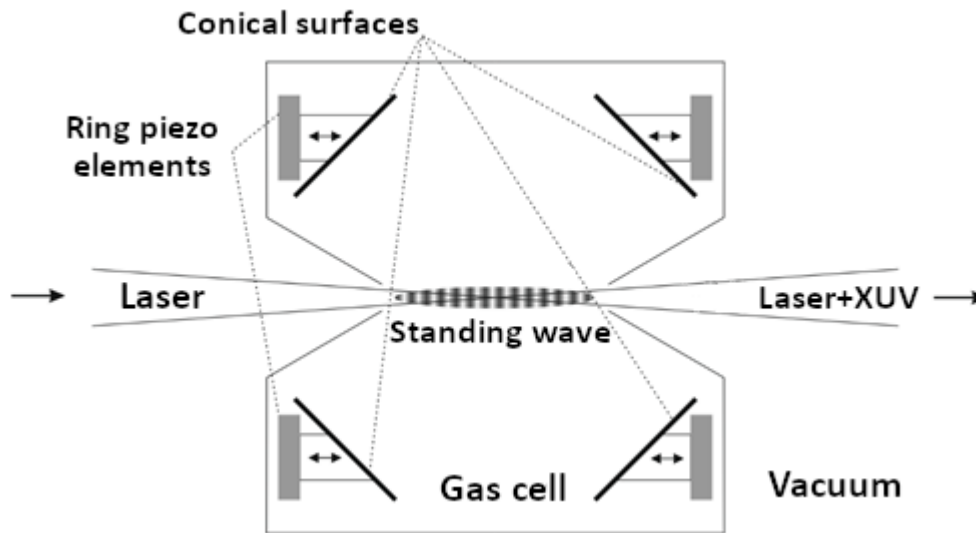


Figure 27: Acoustically density-modulated gas target design

6.2 Gas jets

Another method how to generate gas density modulation is by the series of gas jet nozzles. If we assume the gas plume coming out from the nozzle is homogeneous, the series of such nozzles leads to the step modulation in the cell because there will be

regions in space with the gas pressure from the plume and regions with low pressure in space between the plumes. A configuration with a series of jets close enough to each other is a reasonable approximation of a step-modulated medium. A series of nozzles designed for an experiment is presented in figure 28.

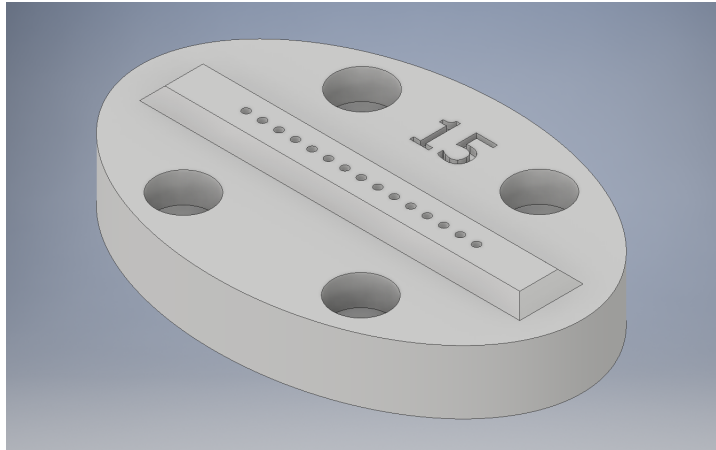


Figure 28: 3D-printed gas jet nozzle for density-modulated target, there are 15 gas jets with the spacing 1.3 mm

The internal design of single nozzle is shown in figure 29.

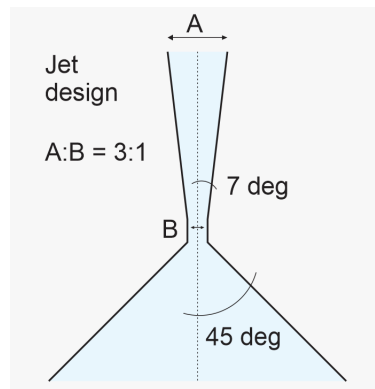


Figure 29: The geometry of single nozzle with $A=600 \mu\text{m}$ and $B= 200 \mu\text{m}$

7 Experimental implementation of density modulated targets

An experiment was conducted in February 2022 at ELI Beamlines. The goal was to achieve spectral selective filtering by QPM in density modulated gas cell with a Bessel-Gaussian beam. The aim of this chapter is to describe the experimental implementation and present the results of the experiment.

7.1 Description of the experimental setup

The original experimental setup is seen in figure 30. Bessel-Gaussian beam was created from Gaussian beam by a set of two axicons. The Ti-sapphire laser working in the pulse regime was focused into the series of gas jet nozzles. The driving field was filtered by the $1,05 \mu\text{m}$ aluminum filter and generated field was diagnosed by the XUV spectrometer. The repetition frequency of the laser was $f_{rep} = 1 \text{ kHz}$ but it was lowered by an optical chopper to $f_{rep} = 100 \text{ Hz}$ in order to fire a single shot with synchronized shutter and prevent damage to optical components. The energy of pulse was $E = 9 \text{ mJ}$ and the duration $\tau = 40 \text{ fs}$. The Gaussian beam was focused by the spherical lens with the focal length $f = 2 \text{ m}$ into the argon gas target. The gas target was composed of 15 gas jet nozzles that were separated by 1.3 mm from each other and the backing pressure was 51 bar . The outer diameter A from picture 29 was $A = 600 \mu\text{m}$ and the inner diameter $B = 200 \mu\text{m}$. The whole setup was placed in a vacuum chambers.

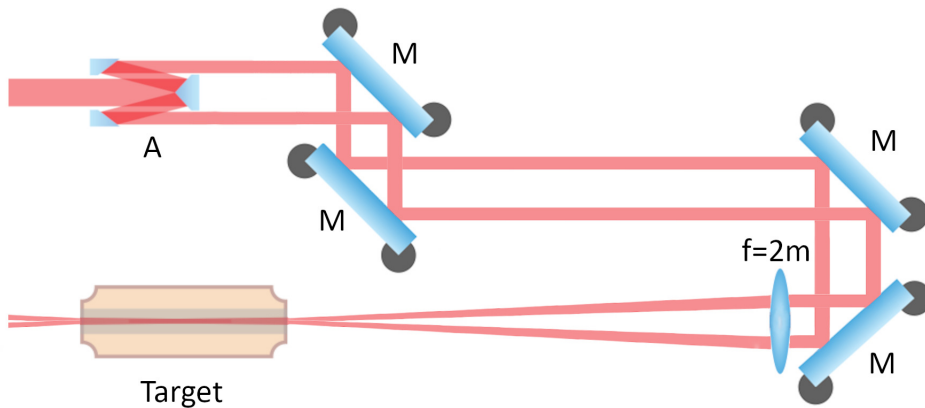


Figure 30: Schematic setup for density-modulated gas target while using Bessel-Gaussian beam, A represents set of two axicons, M mirrors for reflecting the beam into the focus element with focal length $f = 2 \text{ m}$

Unfortunately, this setup could not be used to even generate high harmonic frequencies. This was because of the aberrations of the system that resulted in low intensity in the focus and the intensity was not high enough to ionize the argon atoms. In the end, we used a similar experimental setup with axicons removed using a regular Gaussian beam. This setup is depicted in figure 31.

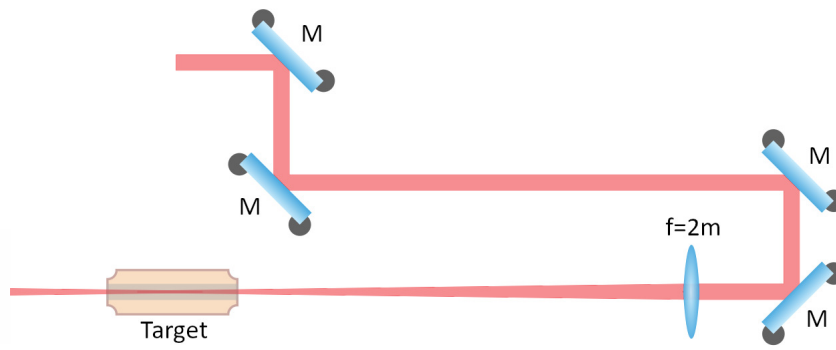


Figure 31: Schematic setup for density-modulated gas target while using Gaussian beam, M are reflecting mirrors and $f = 2$ m spherical mirror

7.2 Results

The results are in the form of camera snapshots from the XUV spectrometer. We shall present 3 series of measurements. The first two series are for 2 positions of the lens x_m and in both positions was changed the diameter of the optomechanical iris d_i to 13 different values. The last series is measured for the third position of the mirror and 5 values of the diameter of the iris. For each value of diameter d_i , were captured 10 single-shots using the XUV spectrometer. An example of one such snapshot is presented in figure 32. The XUV radiation is diffracted on a grating in the horizontal axis that can be converted to the wavelength if the calibration is known and dots represent the high harmonic orders. Graphs with the converted wavelength from the calibration will be used in the following text.

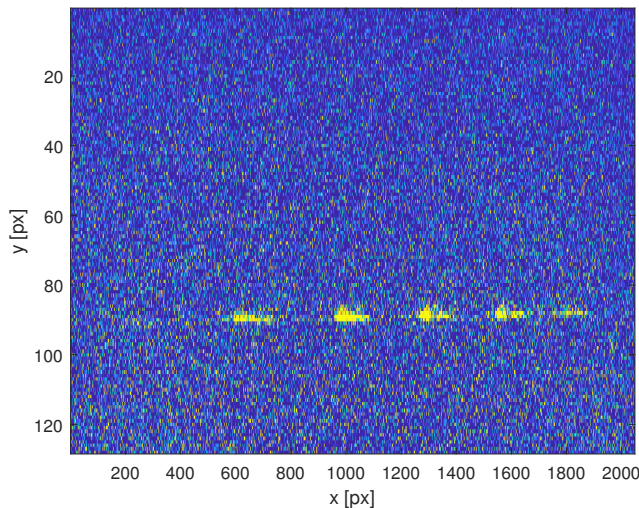


Figure 32: An example of one snapshot from the XUV spectrometer

All 10 images for each value of diameter d_i for a single position of focus were averaged and the values I_{out} on the z axis were plotted. An example of the average of ten snapshots for the diameter of the iris $d_i \doteq 16.6$ mm, relative position of the focusing element $x_m = -41.22$ with the added dependence of intensity I_{out} over the wavelength λ is presented in the figure 33. In this particular example, we can see dominant harmonic order $\lambda_{q=23} = 34.4$ nm. This data processing was done for all 3 series of measurements. Furthermore, we kept the track of the maximal value of intensity I_{out} for each harmonic order. Values of maximum intensity were plotted over the diameter of the iris d_i for the 3 relative positions of the focusing mirror x_m . We can see those plots in figures 34.

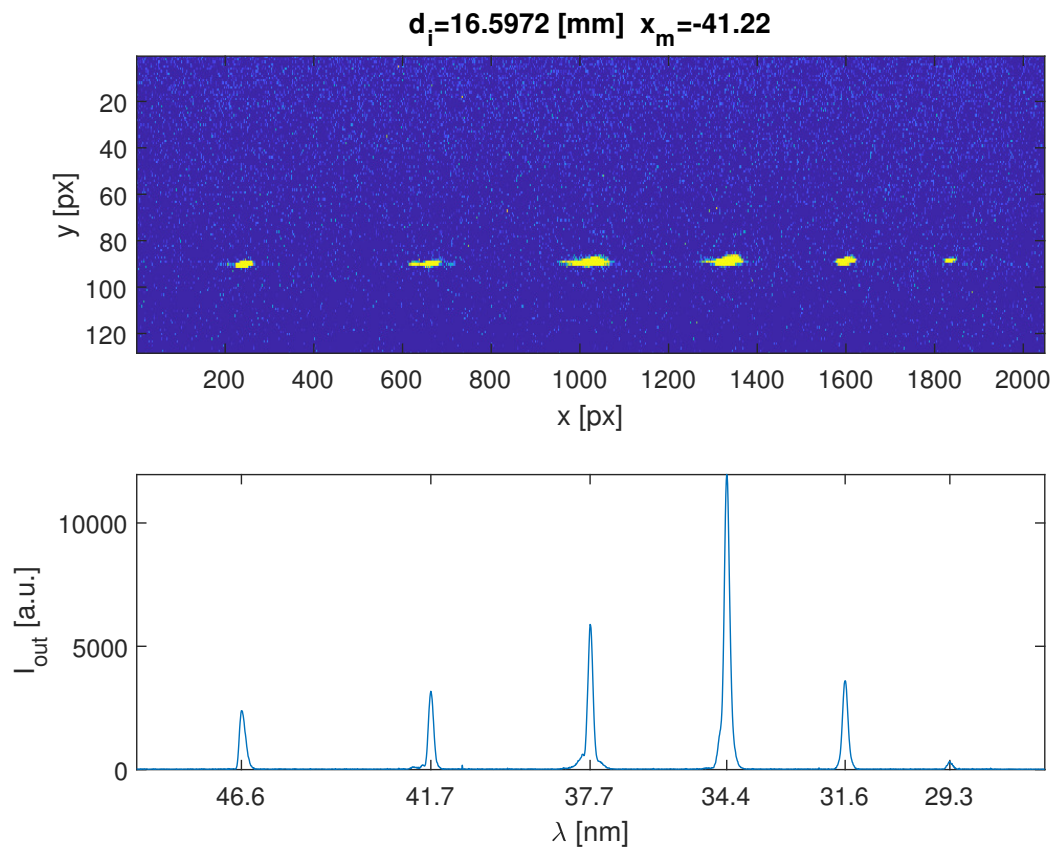
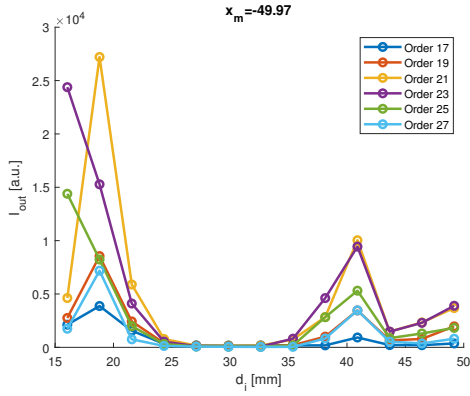
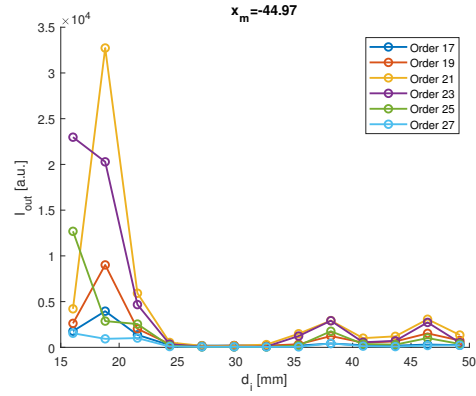


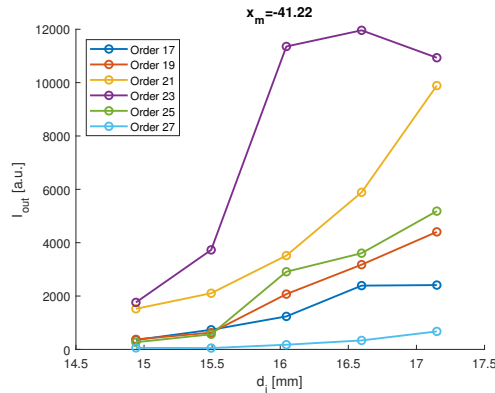
Figure 33: An example of average of 10 images from the spectrometer for the diameter of the iris $d_i \doteq 16.6$ mm and relative position of the focusing element $x_m = -41.22$, the graph below shows the intensity I_{out} of the wavelength λ



(a) Dependence of $I_{out}(d_i)$ for the first series of measurement



(b) Dependence of $I_{out}(d_i)$ for the second series of measurement



(c) Dependence of $I_{out}(d_i)$ for the third series of measurement

Figure 34: Maximum values of I_{out} of generated high harmonic orders over diameter of iris d_i for positions of the focusing mirror x_m

7.3 Conclusions a disscussion

The goal of the experiment was to observe a strong signal of single high harmonic order while others are suppressed in comparison. A scan for the diameter of the optomechanical iris was done because the intensity in the focus changes ionization η in the gas and results from chapter 4 show it is one of the deciding factors for the selective filtering. Originally, the experiment was designed to be conducted with density-modulated targets while using a Bessel-Gaussian beam. High harmonic signal was not generated at all, although we prepared the experimental setup and aligned the BG beam. The reason behind that was a multi-focus spot that had uneven energy distribution. The intensity in the focus was simply not high enough to generate the XUV radiation. After this realization, the experiment was conducted with the Gaussian beam, even though the beam did not have the desired parameters in terms of geometrical wavenumber k_g .

Figures 34 do not show any results that confirm selective filtering. The main reason we did not achieve selective filtering was a laser beam without the specific geometric phase we needed. We also used a gas target in the form of a series of gas jet nozzles, figure 28, and we did not calculate any complex simulations with such target. We could not use the acoustic gas target with the design from figure 27 because we were not able to find a manufacturer who would create piezo elements with our desired parameters. This experiment did not fulfill its goal but it was a huge experience for future experiments with the framework of experimental problems that were not encountered before.

Conclusion and Discussion

This work was dedicated to the process of high harmonic generation in density modulated targets. The first chapter explains the generation on the three-step model along with the phase-matching condition. The three steps are ionization, propagation of electron, and recombination. The biggest factors for phase-matching are the dispersion of neutral atoms, plasma dispersion, dipole dispersion, and geometric dispersion. The second chapter describes the physical model of light propagation in the gas cell. Generated radiation originates at each point of the cell and gains a corresponding phase throughout the space. The third chapter shows the numerical implementation of the code based on the physical model. The code was written in the software MATLAB[®] and consists of the main classes. This code was used to calculate simulations in density-modulated gas targets. The simulations are shown for the sinusoidal and step modulations for argon. The results show that selective filtering can be achieved in the quasi-phase-matching region for a given order. This was the subject of the fourth chapter. The following fifth chapter is about the laser pulse design fulfilling the parameters for selective filtering. The ADK ionization model is used to determine the pulse for the ionization dependence from the simulations. Chapter six presents experimental gas targets eligible for a density modulation. One of them is designed for generating standing acoustic wave on the axis of the laser beam. The second one is a series of gas jet nozzles. The last chapter presents the setup and results of an experiment with a density-modulated gas target conducted at ELI Beamlines in Dolní Břežany.

Reference

- [1] Matěj Dvořáček. *High harmonic generation in gas with standing acoustic wave*. ČVUT FJFI, Praha, 2020. Bachelor’s thesis.
- [2] Matěj Dvořáček. *Quasi-phase matching of high-order harmonic generation on a standing acoustic wave*. ČVUT FJFI, Praha, 2021. Research task.
- [3] V. E. Nefedova, M. F. Ciappina, O. Finke, M. Albrecht, M. Kozlová, and J. Nejd. Efficiency control of high-order harmonic generation in gases using driving pulse spectral features. *Applied Physics Letters*, 113(19):191101, 2018.
- [4] David Attwood. *Soft X-rays and Extreme Ultraviolet Radiation*. Cambridge, Cambridge University Press, 1999.
- [5] Jiří Tolar. *Vlnění, optika a atomová fyzika*. ČVUT, FJFI, 2017.
- [6] Pavel Kwicien. *Základy optiky*. http://optics.fjfi.cvut.cz/files/secured5/ZAOP_prezentace.pdf. [Online; cited April 26, 2022].
- [7] William Putnam, Damian Schimpf, Gilberto Abram, and Franz Kärtner. Bessel-gauss beam enhancement cavities for high-intensity applications. *Optics express*, 20:24429–43, 10 2012.
- [8] Zenghu Chang. *Fundamentals of attosecond optics*. CRC Press, Boca Raton, 2011;2016;.
- [9] V. V. Strelkov and R. A. Ganeev. Quasi-phase-matching of high-order harmonics in plasma plumes: theory and experiment. *Opt. Express*, 25(18):21068–21083, 2017.
- [10] Marek Škereň. *Fyzikální optika*. [Online; cited April 26, 2022].
- [11] Mikhail N. Polyanskiy. Refractive index database. <https://refractiveindex.info>. [Online; cited April 26, 2022].
- [12] Francesco Pampaloni and Joerg Enderlein. *Gaussian, hermite-gaussian, and laguerre-gaussian beams: A primer*, 2004.
- [13] E. Constant, D. Garzella, P. Breger, E. Mével, Ch. Dorrer, C. Le Blanc, F. Salin, and P. Agostini. Optimizing high harmonic generation in absorbing gases: Model and experiment. *Phys. Rev. Lett.*, 82:1668–1671, 1999.
- [14] C. Jin. *Theory of Nonlinear Propagation of High Harmonics Generated in a Gaseous Medium*. Springer Theses. Springer International Publishing, 2013.
- [15] Wikipedia. Trapezoidal rule, 2022. [Online; accessed April 26, 2022].
- [16] Ondřej Finke. *Změny femtosekundového impulzu při generaci vysokých harmonických frekvencí*. ČVUT FJFI, Praha, 2018.

- [17] Maxim V Ammosov, Nikolai B Delone, and Vladimir P Krainov. Tunnel Ionization Of Complex Atoms And Atomic Ions In Electromagnetic Field. 0664:138 – 141, 1986.
- [18] X. M. Tong, Z. X. Zhao, and C. D. Lin. Theory of molecular tunneling ionization. *Phys. Rev. A*, 66:033402, Sep 2002.
- [19] Vábek Jan. *Generace attosekundových impulsů pomocí intenzivního femtosekundového laseru*. PhD thesis, 2014.
- [20] Rüdiger Paschotta. Optical intensity. https://www.rp-photonics.com/optical_intensity.html. [Online; cited April 26, 2022].
- [21] Jean-Claude Diels and Wolfgang Rudolph. *Ultrashort Laser Pulse Phenomena*. 2006.
- [22] Ondřej Jiříček. *Úvod do akustiky*. ČVUT, Praha, 2002.
- [23] Pradip K. Chakrabarti and Satyabrata Chowdhury. *A Textbook on Waves and Acoustics with an Introduction to Mathematical Physics*. New Central Book Agency, La Vergne, 2020.

Appendix

1 Tables

q [-]	η [%]
23	5.09
25	4.77
27	4.54
29	4.36
31	4.23

Table 1: Table of optimal ionizations η for the orders 23 to 31 q in argon

	Density rho $\left[\frac{kg}{m^3}\right]$	Speed of sound c $\left[\frac{m}{s}\right]$
Ar	1.76	319
Kr	3.69	221
He	0.18	1007
Ne	0.89	435
Xe	5.76	178

Table 2: Table of densities of noble gases and speed of sound in noble gases defined as properties in the class sound2

2 MATLAB® Codes

Code hhg82gf.m

```
1 classdef hhg82gf
2     properties
3         c = 299792458; %Speed of light in vacuum [m/s]
4         eps0 = 8.854187817e-12; %Permittivity of vacuum [F/m]
5         p_a = 101325; %Atmospheric pressure [pa]
6     end
7
8     methods
9         function z_r=rayleigh(obj,lambda,fc,d)
10            %Function to calculate the Rayleigh's length
11            %                lambda is the wavelength [m]
12            %                fc is the focal length of the mirror [m]
13            %                d is the diameter of the beam on the mirror [m]
14
15            F=fc/d; %F-number
16            z_r=(lambda)/(pi)*(1)/(atan(1/(2*F)^2));
17
18        end
19
20        function signal(obj,gas,N,q,L,lambda,p,eta,modulation,A,fr,x,gf)
21            %HHG signal for case with no pressure modulation , amplitude neglected
22            %Input parameters: Gas is the type of used noble gas, 'Ar'/'Kr'/'He'/'Xe'/'Ne
23            %                N is amount of points where HH signal is generated [-]
24            %                q is order of high harmonic [-]
25            %                L is length of medium [m]
26            %                lambda is the wavelength of used laser [m]
27            %                p is the pressure of the gas in the cell [bar]
28            %                eta is the percentage of the ionized particles, input is
29            %                in the form 0.04 for 4%, eta input is in [0,1] [-]
30            %                modulation is the modulation of pressure, 'sin(x)' or 1
31            %                for no modulation
32            %                A is the amplitude of the standing sound wave, it is the
33            %                percentage of the mean value of gas pressure, A input is in [0,1] [-]
34            %                fr is the frequency of the standing sound wave [Hz]
35            %                fc is the focal length of the mirror [m]
36            %                d is the diameter of the beam on the mirror [m]
37            %                x is the distance of the beam waist from the origin of the
38            %                cell [m]
39
40            z=linspace(0,L,N);
41            N_z=length(z);
42            lambda_q=(1)/(q).*lambda;
43            s=MedClass;
44            b=sound2;
45            dz = z(2)-z(1);
46            neu = 1-eta;
47
48            fi=zeros(1,N_z);
49            E_q=zeros(1,N_z);
50            I=zeros(1,N_z);
51            pom0=zeros(1,N_z);
52            f=zeros(1,N_z);
53            g=zeros(1,N_z);
54
55            pressure=b.modulation1(gas,N,L,p,modulation,A,fr); %Pressure modulation
56
57            poms0=s.sPlasma(eta,lambda);% Susceptibility of plasma for laser radiation
58            poms1=s.sDriver(gas,lambda);% Susceptibility of neutrals for laser
```

```

59     radiation
60     poms2=s.sPlasma(eta,lambda_q);% Susceptibility of plasma for HH signal
61     poms3=s.sXuv(gas,lambda_q);% Susceptibility of neutrals for HH signal
62
63     for j=1:N_z
64         f(1,j)=(2*pi)./(lambda).*sqrt( pressure(j)/(obj.p_a).*(poms0+neu*poms1)+1)
65         -gf;
66         %Integrand of the first integral int(k_0(z)dz)_0^(z_n) from the gathered
67         phase fi in the medium
68
69         g(1,j)=(2*pi)./(lambda_q).*sqrt( pressure(j)/(obj.p_a).*(poms2+neu*poms3)
70         +1)+obj.dipole(z(j),z_R,x);
71         %Integrand of the second integral int(k_0(z)dz)_0^(z_n) from the gathered
72         phase fi in the medium
73
74     end
75
76     fp=cumtrapz(z,f);
77     gp=cumtrapz(z,g);
78     %Integrals of the wave vectors
79
80     %The average value of attenuation length
81     atlaverage=s.aLength(gas,lambda_q,p);
82
83     for j=1:N_z
84         fi(1,j)=q.*(fp(j)-fp(1))+gp(N_z)-gp(j);
85         %Gathered phase
86
87         E_q(1,j)=exp(-1*(L-z(N_z-j+1))/(2*atlaverage))*exp(1i*fi(1,j))*dz;
88         %Definition of newborn field
89
90     end
91
92     pom=0;
93
94     for j=1:N_z
95         %Auxilliary variable that keeps the values to calculate intensity in
96         each point
97         %I=|E|^2
98         %E=sum(exp(i*fi_k))_(k=1)^n - Intensity in each point z_n will be the
99         sum of the fields to that point
100        %I.e. for point z_3 the field will be E=exp(i*fi_1)+exp(i*fi_2)+exp(i*
101        fi_3)
102        %
103        %           z_2 the field will be E=exp(i*fi_1)+exp(i*fi_2)
104        %           z_1 the field will be E=exp(i*fi_1)
105
106        pom0(1,j)=pom+E_q(1,j);
107        pom=pom0(1,j);
108    end
109
110    for j=1:N_z
111        I(1,j)=abs(pom0(1,j)).^2;
112        %Calculating intensity in each point z_n
113    end
114
115    %figure
116    plot(z,I)
117
118    title(jmeno)
119    xlabel ('z [m]')
120    ylabel ('I_{out} [a.u.]')

```



```

119
120
121
122     end
123
124     function dip=dipole(obj,z,z_r,x)
125         %Function to calculate the derivative (gradient) of the dipole phase  $K=\text{grad}$ 
126         %           (fi_D),  $\text{fi}_D=-\alpha \cdot I$ 
127         %           z is the point of space where we calculate the dipole
128         %           moment, the distance from the origin of the cell [m]
129         %           z_r is the Rayleigh's length [m]
130         %           x is the distance of the beam waist from the origin of the
131         %           cell [m]
132         %           There is preset a mean value of laser intensity  $I_0$ 
133         %            $=2 \cdot 10^{18}$  W/m2 and the proportional constant for short trajectories
134         %            $\alpha=10^{-18}$  m2/W
135         dip=(10-(18)*10-(18))*2*(z_r(2))*2*(z-x)/((z_r2+(z-x)2)(2));
136     end
137 end
138 end

```

Code sound2.m

```

1  classdef sound2
2      properties
3          p_a = 101325; %Atmospheric pressure [pa]
4          rho_ar=1.7572; %Densities of noble gases [kg/m3], taken from - http://www.converter.cz/tabulky/hustota-plynu.htm
5          rho_kr=3.69;
6          rho_he=0.1761;
7          rho_ne=0.888;
8          rho_xe=5.761;
9          cNeon=435; %Speed of sound in various gases [m/s]
10         cHelium=1007;
11         cXenon=178;
12         cArgon=319;
13         cKrypton=221;
14     end
15
16     methods
17         function pressureS=modulation1(obj,gas,N,L,p,modulation,B,fr)
18             %Function to calculate pressure as numerical vector in case of modulation
19             %that depends on length of the media
20
21
22             if(isnumeric(modulation)==0)
23                 modulation=char(modulation);
24             end
25
26
27             if(gas=='Ne')
28                 cz=obj.cNeon;
29             elseif(gas=='Ar')
30                 cz=obj.cArgon;
31             elseif(gas=='He')
32                 cz=obj.cHelium;
33             elseif(gas=='Xe')
34                 cz=obj.cXenon;
35             elseif(gas=='Kr')
36                 cz=obj.cKrypton;
37             end
38
39
40             omega=2*pi*fr;
41             k0=omega/cz;
42
43

```

```

44     switch modulation
45         case (1)
46             z1=linspace(0,L,N);
47             N_z1=length(z1);
48             pressureS=zeros(1,N_z1);
49             pom1=zeros(1,N_z1);
50             B=1;
51             for i=1:N_z1
52                 pressureS(1,i)=(p*10^5+(p*10^5)*B*pom1(i));
53             end
54         case ('sin(x)')
55             z1=linspace(0,L,N);
56             N_z1=length(z1);
57             pressureS=zeros(1,N_z1);
58             pom1=sin(k0*z1);
59             for i=1:N_z1
60                 pressureS(1,i)=(p*10^5+(p*10^5)*B*pom1(i));
61             end
62         case ('step')
63             z=linspace(0,L,N);
64             pressureS = p*10^5+B*p*10^5.*sign(sin(k0.*z));
65     end
66
67     end
68
69     end
70
71     end

```